UNIVERSITY OF
Southampton
Institute of Sound and
Vibration Research

ISVR Technical Memorandum

Anechoic wind tunnel tests on high-speed train bogie aerodynamic noise

E. Latorre Iglesias and D.J. Thompson

ISVR Technical Memorandum No. 1001

May 2014

SCIENTIFIC PUBLICATIONS BY THE ISVR

Technical Reports are published to promote timely dissemination of research results by ISVR personnel. This medium permits more detailed presentation than is usually acceptable for scientific journals. Responsibility for both the content and any opinions expressed rests entirely with the author(s).

Technical Memoranda are produced to enable the early or preliminary release of information by ISVR personnel where such release is deemed to the appropriate. Information contained in these memoranda may be incomplete, or form part of a continuing programme; this should be borne in mind when using or quoting from these documents.

Contract Reports are produced to record the results of scientific work carried out for sponsors, under contract. The ISVR treats these reports as confidential to sponsors and does not make them available for general circulation. Individual sponsors may, however, authorize subsequent release of the material.

UNIVERSITY OF SOUTHAMPTON

INSTITUTE OF SOUND AND VIBRATION RESEARCH

DYNAMICS GROUP

Anechoic wind tunnel tests on high-speed train bogie aerodynamic noise

by

E. Latorre Iglesias and D.J. Thompson

ISVR Technical Memorandum No. 1001

May 2014

Authorised issue by
Prof. D.J. Thompson

Acknoledgements

The work presented in this report was carried out during a six month placement at the Railway Technical Research Centre (RTRI) located in Tokyo, Japan, under the *Pre/Postdoctoral Fellowship for Foreign Researchers (Short Term)* Award given by the Japan Society for the Promotion of Science (JSPS). The author is grateful to JSPS for the funding provided and to the RTRI for making the Maibara anechoic wind tunnel available and for all the valuable support provided.

Contents

Abstract

When trains run at high speed, aerodynamic noise sources become important. Of the various sources, the bogie region is one of the most difficult to model as both the flow field and the geometry are complex. Moreover, it is difficult to use experimental techniques on a running train to separate aerodynamic noise from rolling noise. Wind tunnel tests can be used as an alternative to field tests in order to assess the aerodynamic noise radiated by the bogie components or by the bogie itself.

Experiments on the noise radiated by a 1/7 scale model of a simplified high-speed train bogie were carried out in the Railway Technical Research Institute (RTRI) anechoic wind tunnel at Maibara, Japan. The bogie mock-up was installed in the bogie cavity of a 1/7 scale model of a high-speed train car body in order to approximate the same flow conditions as found on a full scale high-speed train. The noise measurements were carried out using a microphone array. Additionally seven omnidirectional microphones were used to measure directivity, covering different radiation angles upstream and downstream of the bogie position.

Two flow configurations were used representing those measured experimentally by RTRI during field tests at the inlet of the rear bogie cavity of the first (leading car) and fifth (middle car) cars of a full-scale high-speed train. In both cases the flow speed profiles at the bogie cavity inlet of the 1/7 scale mock-up were adjusted to those measured at the inlet of the full-scale bogie cavity. A range of flow speeds between 180 and 360 km/h were studied in order to assess the dependence of the bogie aerodynamic noise on the train speed.

The effect of internal components within the bogie was studied using three different configurations representing a motor bogie, a trailer bogie and a simple bogie frame without wheelsets. It was found that the shielding effect of the bogie cavity is decisive for the noise radiated by the bogie components, due to the reduction of the incident flow speed.

The influence of the side components of the bogie was assessed by extending the bogie side frame laterally by three different lengths and also using cavity side covers, in an attempt to understand the importance of the relative position of the lateral components with respect to the bogie cavity. This arrangement allows the results to be applied to different high-speed train geometries.

The directivity obtained when the wheel shafts were extended by 100 mm was very close to that expected for an omnidirectional source and it was similar for the different flow speeds. The directivity obtained with this configuration is assumed to be comparable to the directivity of the bogie itself but the influence of the relative position between the side components and the bogie cavity and the train body was not assessed.

The results of the experiments provide a good framework for the validation of prediction models for the noise radiated by a high-speed train bogie as well as investigating the dependence on the various factors that affect the bogie aerodynamic noise generation.

List of symbols

c_0	Speed of sound (m/s)
d	Distance between the noise source and the receiver (m)
I	Sound intensity (W/m^2)
R_i	Distance between the bogie centre and the i- microphone (m)
R_0	Distance between the bogie centre and the reference microphone (m)
S	Surface area (m^2)
U	Mainstream flow speed (m/s)
$U_{leading}$	Local mean flow speed for the leading car flow conditions (m/s)
U_{middle}	Local mean flow speed for the middle car flow conditions (m/s)
U_0	Mean flow speed (m/s)
α	Speed exponent
ΔS	Ratio of the surface area
ΔSPL	Increment of the Sound Pressure Level (SPL) (dB, re 2×10^{-5} Pa)
ΔU	Ratio of the incident flow
ρ_0	Air density (kg/m^3)

1 Introduction

When trains run at sufficiently high speeds, aerodynamic noise becomes a predominant noise source. The bogie region is one of the most relevant aerodynamic noise sources in high-speed trains. It is important to assess the aerodynamic noise from the bogie in order to validate numerical models or calibrate them, as is the case for empirical or semi-empirical models, which rely on experiments. The complexity of the geometry of the bogie and the flow field in the bogie region makes it difficult to model it.

The use of experimental techniques in field tests has the drawback that it is difficult to separate the aerodynamic noise from the rolling noise. As an alternative, wind tunnel test can be used to evaluate the aerodynamic noise from train bogies. In order to minimise the background noise from the wind tunnel itself and the effect of the sound reflections with the walls of the wind tunnel, open-section anechoic wind tunnels are preferred for aeroacoustic measurements. Microphone arrays are extensively used in order to increase the signal to noise ratio, in this particular case to minimize the effect of noise sources other than the bogie, and to obtain noise maps for noise source localization within the bogie region.

In the present work, noise tests have been carried out in the RTRI open-section anechoic wind tunnel located at Maibara (Japan) using a 1/7 scale bogie mock-up installed in the bogie cavity of a 1/7 scale high-speed train car model. A microphone array combined with beamforming techniques was used for both obtaining the noise spectrum radiated by the different bogie configurations and obtaining the noise maps for noise source localization. Due to the limited time available to perform the tests, the directivity measurements were carried out using seven omnidirectional microphones placed on a strut parallel to the flow direction, instead of using the microphone array.

Experiments are presented in this report that try to give an experimental framework to validate and calibrate empirical and numerical prediction models. Moreover, it is also intended to investigate the dependence on the various factors that affect the aerodynamic noise generation not only from the whole bogie but also from the different bogie components.

Curle has shown that the noise generated by the interaction of an incoming air flow and a solid body is equivalent to a distribution of dipole sources on the body's surface [1]. After applying a dimensional analysis it was shown that the sound intensity radiated by the dipole sources in the acoustic far-field is proportional to $I \propto \rho_0 U_0^{\alpha} S d^{-2} c_0^{-3}$ where ρ_0 is the air density, U_0 is the mean flow speed, α is the speed exponent, S is the surface area of the solid immersed into the air flow, d is the distance between the noise source and the receiver and c_0 is the speed of sound [1].

The case of a train bogie when the train runs at a certain speed can be equivalent to the case of a bluff body immersed in an air flow. The aerodynamic noise will be produced by the air flow interaction with the different bogie components and the aerodynamic noise generated by the fluctuating forces on the surface of the bogie components can be described by equivalent dipole sources. Therefore, the aerodynamic noise radiated by the bogie will rely on the speed of the incident flow and the surface area of the components exposed to that flow. In that sense, the relative position of the bogie components with respect to the bogie cavity will determine the noise radiation due to the screening effect of the upstream step of the bogie cavity. The components located inside the cavity will be shielded by the upstream step of the cavity and the incident flow speed will be reduced, leading to a reduction of the noise radiation. In the same way, the rear components of the bogie will be shielded by the leading components, reducing the incident flow

speed that they experience.

According to this, the components that lie below the upstream step of the cavity are expected to be noisier than those inside the cavity. It is interesting to assess the relative position of the bogie components not only at the centre of the cavity, but also at the sides of it. The latest types of Japanese high-speed train Shinkansen use side covers that avoid the air flow from reaching the lateral components of the bogie, reducing the incident flow speed and consequently the noise radiation. In contrast, in most European high-speed trains, the bogie cavity is open and the lateral components of the bogie are exposed to a side flow with a higher incident speed. The relative position of the bogie side component inside the bogie cavity is also different for the different high-speed train models. For this reason, the contribution of the side components to the overall aerodynamic noise radiated by the bogie needs to be assessed. The surface area of the components exposed to the side flow and the incident flow speed seem to be the parameters that may alter the noise radiation, according to Curle's theory. The experimental results are simplistically compared to the expected theoretical results.

The position of the bogie along the train will influence the noise radiation as the flow is decelerated downstream of the train nose by the friction with the train surface (boundary layer) and by the interaction with different bluff bodies, as for example the components of different bogies located upstream. The use of scale models, with a shorter distance between the train noise and the position of the bogie, leads to different flow speed at the inlet of the bogie cavity. In this regard, the flow speed profiles at the inlet of the bogie cavity have been adjusted to correspond to those measured experimentally at the inlet of the rear bogie cavity of the first (leading car) and fifth (middle car) car of a real high-speed train during field tests [2], in an attempt to have the same flow conditions in the wind tunnel tests compared to the real case. This approach also compensates the fact that a moving ground was not used during the wind tunnel tests considering that the same flow speed profiles as measured in the real case were obtained using a fixed ground plate.

Due to the complexity of the flow behaviour around the bogie region, the speed dependence of the aerodynamic noise from the bogie may differ from that for an ideal dipole source. The speed dependence of the noise radiated by the bogie itself and by the side components of the bogie have to be assessed to check if it is correctly described by a speed exponent of 6, as expected for a pure dipole source, or if the speed exponent is different. For this reason, all the tests have been performed at four different flow speeds: 180, 275, 320 and 360 km/h. If the length of the side frame is take as the reference, a Reynolds number range between 1.6×10^6 and 3.2×10^6 was covered during the experiments.

The directivity of the bogie aerodynamic noise has to be defined. Unlike the directivity of an isolated dipole source, the geometrical complexity of the bogie and the effect of its location inside the bogie cavity may alter the directivity pattern. Due to the limitation on the time available to carry out the tests, the microphone array could not be used for the directivity measurements so they were carried out by using individual omnidirectional microphones. The signal-to-noise ratio has to be increased then by extending the wheel shafts so the noise generated by the side components of the bogie is high enough compared with the background noise. In this case, the relative position between the side components and the cavity may alter the resultant directivity but it is considered that the results obtained are representative of the directivity of the bogie itself.

2 Experimental set-up

Experiments on the noise radiated by a 1/7 scale model of a simplified high-speed train bogie were carried out in the Railway Technical Research Institute (RTRI) anechoic wind tunnel at Maibara, Japan. The bogie mock-up was installed in the bogie cavity of a 1/7 scale model of a high-speed train car body. Different bogie and flow configurations have been used. The set-up is described in detail in this Section.

2.1 Train and bogie mock-ups

A 1/7 scale mock-up of a simplified bogie was designed for the wind tunnel tests. Two different configurations of the bogie model were built to depict a simplified trailer and motor bogie, as shown in Figure 1. The trailer bogie is composed of the front and rear brake systems, with three brake disks each made of rigid plastic, while the motor bogie has an upstream and downstream motor and gear box made of wood. These components together with the wheels (also made of rigid plastic), which are attached to the wheel shafts, are defined as interior components because they are placed between the side frames. Both side frames and shafts are made of aluminium. The design of the bogie mock-up allows the side frames to be removed and the components attached to the wheel shafts to be changed. Therefore, the side frames could be used separately or combined with the bogie components to form the trailer and the motor bogie configurations.

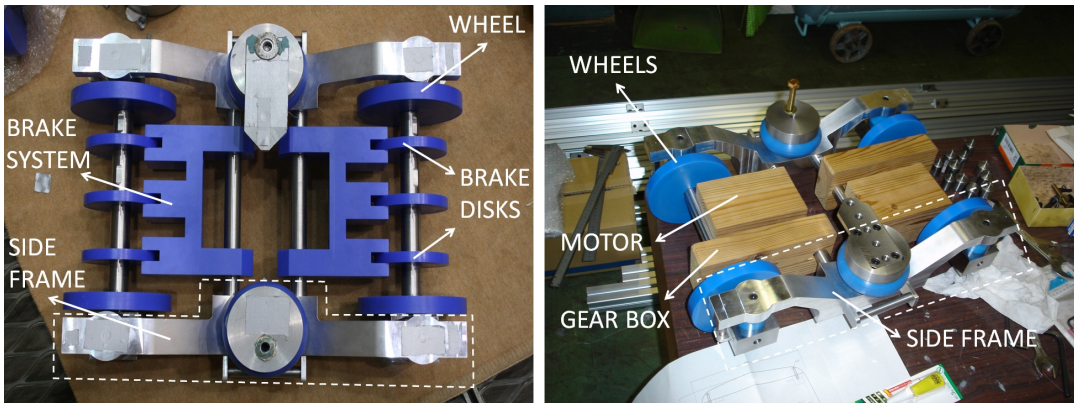

(a) (b)

Figure 1: 1/7 scale simplified bogie mock-up. (a) Trailer bogie. (b) Motor bogie.

In order to assess the contribution to the overall noise of the components placed on the side part of the bogie (hereafter called side components) the wheel shafts were extended allowing one of the side frames to be moved laterally. Three different shaft extensions were used: 50, 75 and 100 mm. Figure 2 shows two different views of the motor bogie when the axles were extended by 100 mm.

The bogie mock-up was attached to the bogie cavity of a 1/7 scale high-speed train car model. The original cavity had both upstream and downstream edges with a sharp shape. In previous experimental studies carried out in the same wind tunnel using a similar set-up it was found that the noise produced by the interaction between the downstream cavity edge and the incident turbulent flow produced after the flow separation at the upstream cavity edge had a significant

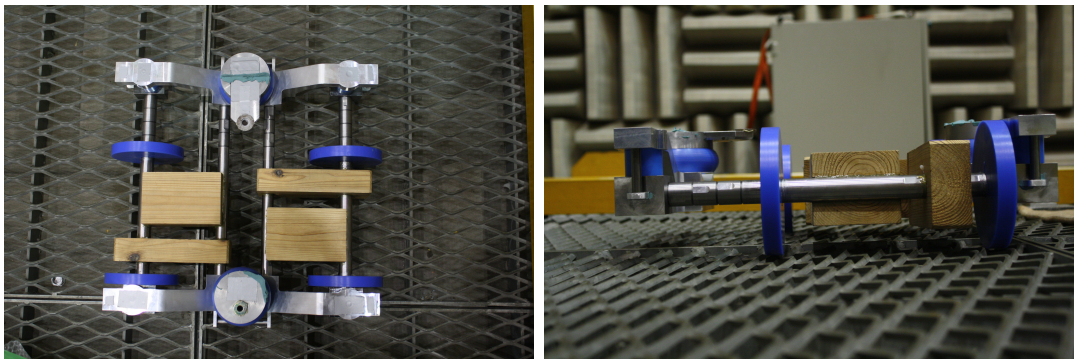

(a) (b)

Figure 2: Motor bogie mock-up with the wheel shafts extended by 100 mm. (a) Top view. (b) Front view.

contribution to the overall noise [3]. Because the aim of the tests presented here is to measure the noise radiated by the bogie itself under flow conditions as they are in the real case, the upstream cavity edge was kept as it was in the initial configuration, but the downstream edge was rounded in an attempt to decreased the interaction noise produced as described above. Figure 3 shows the original sharp downstream edge of the cavity and the rounded version of it.

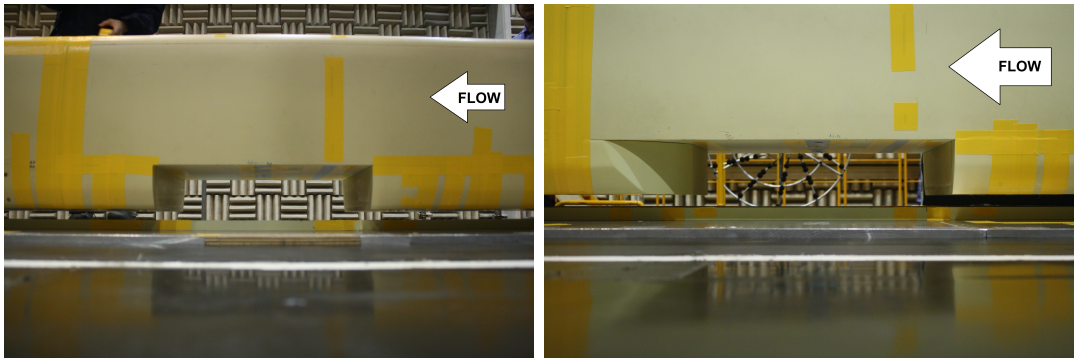

(a) (b)

Figure 3: Two different configurations of the downstream edge of the bogie cavity. (a) Sharp edge. (b) Rounded edge.

Figure 4 (a) and (b) shows the side view of the trailer and the motor bogie when installed in the cavity of the 1/7 scale train model. Figure 4 (c) shows the motor bogie installed inside the bogie cavity but with the full side covers attached as they are in most of the recent Japanese Shinkansen trains. Figure 4 (d) shows just both side frames installed inside the bogie cavity.

2.2 Set-up for the measurements with the microphone array

Figure 5 shows a general view of the experimental set-up used for the noise measurements with the microphone array. The 1/7 scale train car body was attached to a reflective ground the vertical position of which could be changed. The bogie was attached to the only bogie cavity available

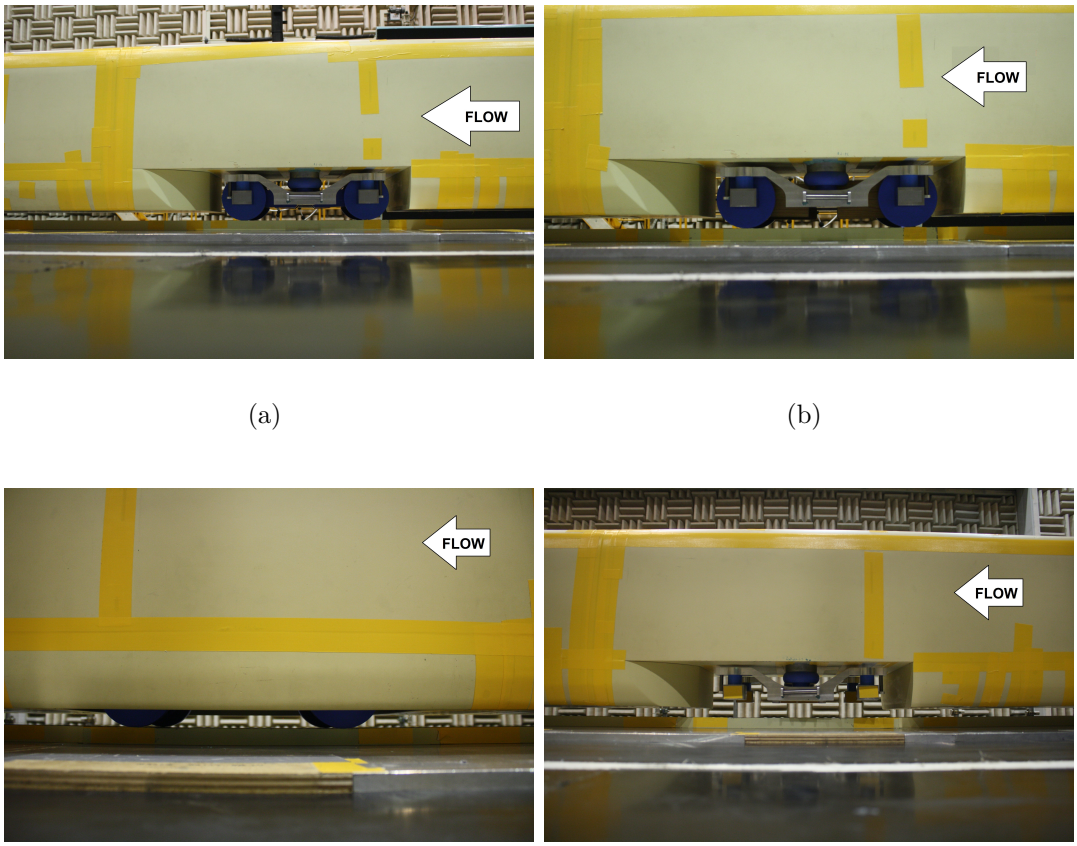

(a) (b)

(c) (d)

Figure 4: Side view of the bogie mock-up installed in the bogie cavity. (a) Motor bogie. (b) Trailer bogie. (c) Motor bogie with full side skirts. (d) Just side frames.

in the train car mock-up. The wind tunnel open section was located inside an anechoic chamber of dimensions 20 m x 22 m x 13 m. More details about the characteristics of the Maibara open section anechoic wind tunnel were published by Maeda and Kondo [4]. A microphone array was used in order to increase the signal-to-noise ratio, defined as the ratio between the noise radiated by the bogie and by the other noise sources present in the experiments (e.g. bogie cavity, train nose, wind tunnel self-noise...). In addition, a noise barrier was installed between the microphone array and the nose of the train in order to minimize the influence of noise sources located in that area. An omnidirectional microphone was placed in the geometrical centre of the microphone array and was used as reference microphone.

Figure 6 shows more details of the experimental set-up. The centre of the microphone array was moved 392 mm downstream with respect to the geometrical centre of the bogie model to account for the flow convection effects. The downstream displacement of the array was calculated for a flow speed of 320 km/h by using the method proposed by Amiet [6]. The distance between the centre of the bogie and the centre of the microphone array was 3.50 m and the centre of the bogie was placed 3.75 m downstream of the nozzle.

Figure 7 shows the microphone array used, which was formed of 66 microphones. The diameter of the outer circumference was 1 m and the height of the centre of the array with respect to the reflecting ground plane on which the train model was installed was 0.5 m, ensuring that none of

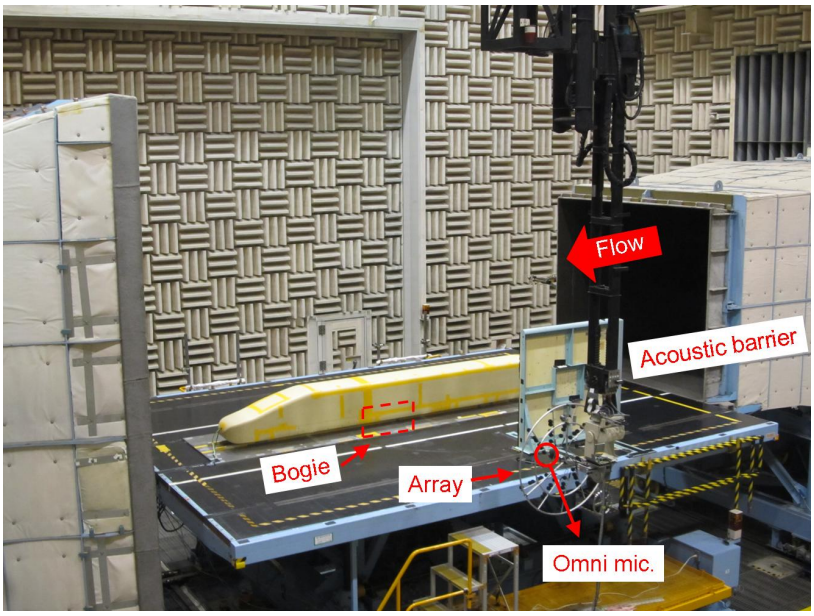

Figure 5: General view of the experimental set-up for the microphone array configuration.

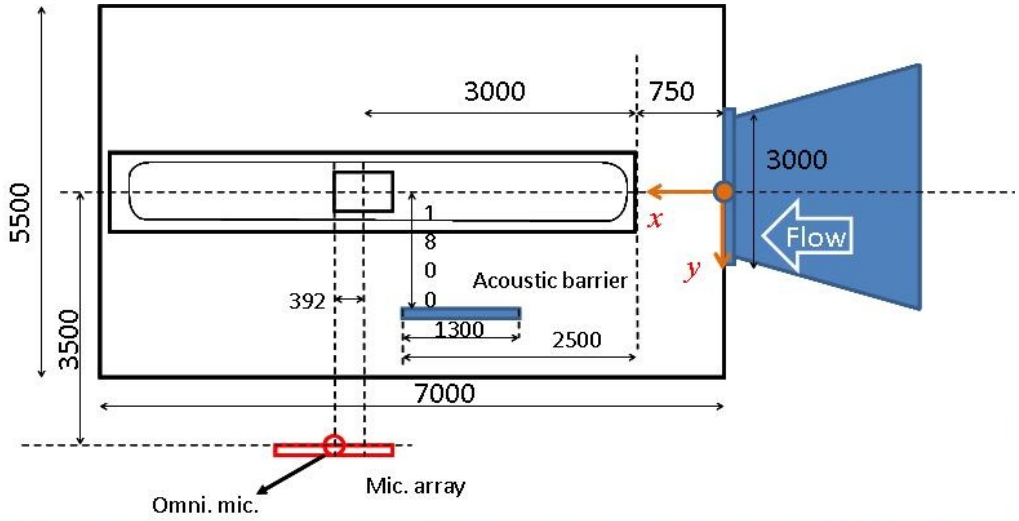

Figure 6: Sketch of the experimental set-up for the microphone array configuration.

the microphones was shielded by the ground. A camera was attached on the array frame in order to obtain the images necessary to match with the noise maps for the different tests.

These 66 microphones were connected to the front-end PULSE 3560D that was in turn connected to a PC using a Gigabit Ethernet hub. The Camera installed on the microphone array was connected directly to the PC. The time acquired for each of the input channels was 4.031 seconds with a sampling frequency of 65,536 Hz. For the case of the independent omnidirectional microphone placed at the centre of the array the time signals were acquired using a multi-track SONY SIR-3000 data recorder with a sampling frequency of 48 kHz and an acquisition time of 20 seconds. Simultaneously, the data was processed in real-time and recorded using the FFT analyzer OnoSokki DS-2000, which provides FFT and 1/3 octave analysis.

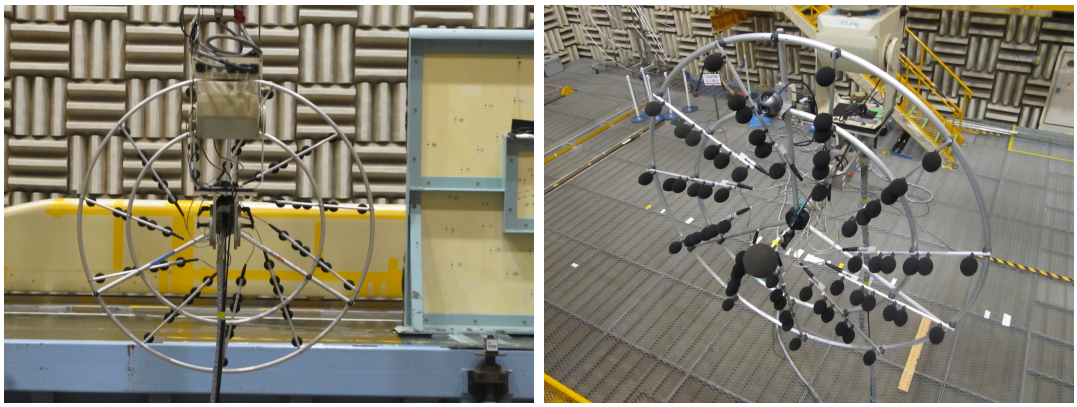

(a) (b)

Figure 7: View of the microphone array used during the measurements. An omnidirectional microphone was placed on the centre of the array to perform independent analysis.

2.3 Set-up for the directivity measurements

The microphone array was not used for the directivity measurements due to the limited time available. In order to cover different radiation angles the position of the microphone array should be changed. The microphone array must be calibrated for each of the measurement positions and the results obtained are very sensitive to the correct alignment of the array with respect to the bogie centre. For this reason, instead of the microphone array, seven omnidirectional microphones were installed on a long strut parallel to the flow direction, as shown in Figure 8. These were installed on the opposite side of the train to the microphone array.

The fact of using omnidirectional microphones makes it critical to obtain a good enough signal-to-noise ratio between the noise radiated by the bogie and other existing noise sources. To maximize the signal-to-noise ratio the bogie wheel shafts on the side closer to the microphones were extended by 100 mm. The acoustic barrier, which was on the opposite side, was removed to avoid unwanted sound reflections.

It is assumed that the directivity of the noise radiated by the side components when the side flow is impinging on them is representative of the directivity of the noise radiated by the bogie itself, as the physical mechanisms involved in the noise generation are the same for all the bogie components. However, the effect of the position of the bogie inside the cavity may alter the actual directivity. This effect is difficult to estimate and it was not accounted for.

Figure 9 shows additional details about the experimental set-up for the directivity measurements. Two different microphone configurations were used. In the first configuration the microphones were located at fixed angle steps of 15°, taking as 0° the line perpendicular to the flow direction passing through the bogie centre, covering a range between $-45°$ and $+45°$ where negative angles represent positions upstream of the bogie centre, as shown in Figure 8. Due to the effect of the convection of the sound inside the jet the actual angles defined by the path followed by the sound propagated from the bogie to each of the microphones will differ from those followed with no flow. For this reason, the corrections proposed by Amiet [6] to include the effect of the sound convection due to the air flow were taken into account to define the microphone positions for the

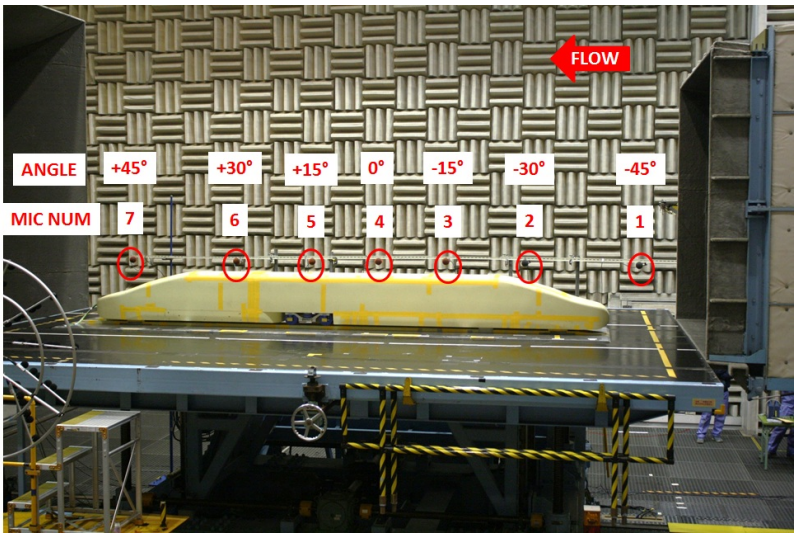

Figure 8: General view of the experimental set-up for the directivity measurements.

second microphone configuration. This correction was only applied to the case of a flow speed of 320 km/h. For both microphone configurations the height of the microphones with respect to the ground plane was 0.5 m.

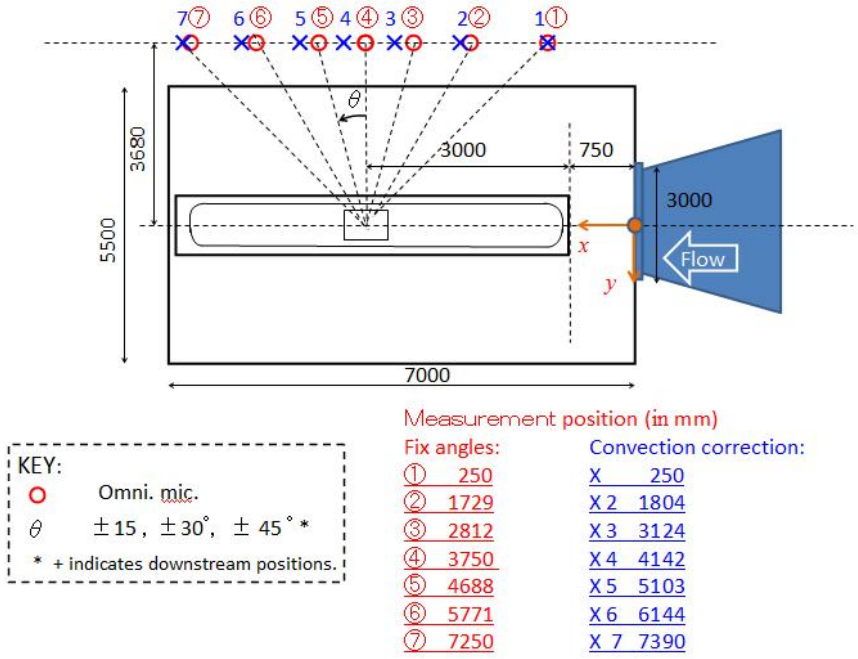

Figure 9: Sketch of the experimental set-up for the directivity measurements.

2.4 Flow configurations

The flow speed profiles at the bogie cavity inlet were measured using a rake of Pitot tubes, as shown in Figure 10. This arrangement allows the local flow speed to be measured at different distances from the train floor (distances between 1 and 53.5 mm from the train floor with steps of 7.5 mm) and at different distances from the centre of the bogie cavity (from 0 to 244 mm in

steps of 56 mm). As flow symmetry was assumed, the speed velocity profiles were measured only at one side of the train model.

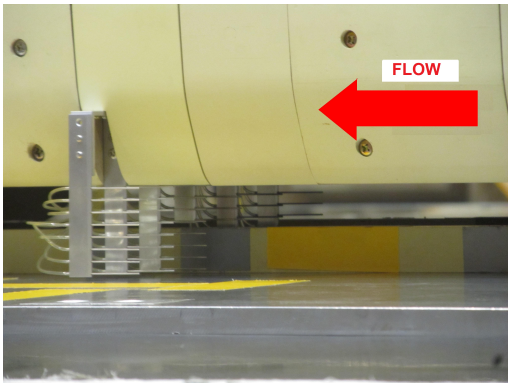

Figure 10: Rake of Pitot tubes used to measure the flow speed profiles at the bogie cavity inlet.

In terms of flow speed profiles two different configurations were used during the tests representing leading and middle car flow configurations. The flow underneath the train body was modified in order to achieve a speed profile as similar as possible to the profiles measured during a field test campaign at the bogie cavity inlet of the rear bogie of the first car (leading) and the rear bogie of the fifth car (middle) of a full scale train [2].

Because the distance covered by the flow from the front part of the train to the bogie cavity inlet is shorter in the case of the 1/7 scale train mock-up compared with the full-scale train the flow has to be decelerated. For the leading car case this was obtained by attaching two elliptical pieces to the rails upstream of the bogie, broadening the rails at those positions, as shown in Figure 11. In the case of the middle car configuration no extra pieces were added to the rails and the flow was slowed down by lowering the ground plate 175 mm relative to the bottom edge of the nozzle, as shown in Figure 12. Just to clarify, the two elliptical supports that appear in Figure 12 (a) are the attachment points between the train and the ground. These supports were used in all the experiments and they are different to those shown in Figure 11 (a) and (b).

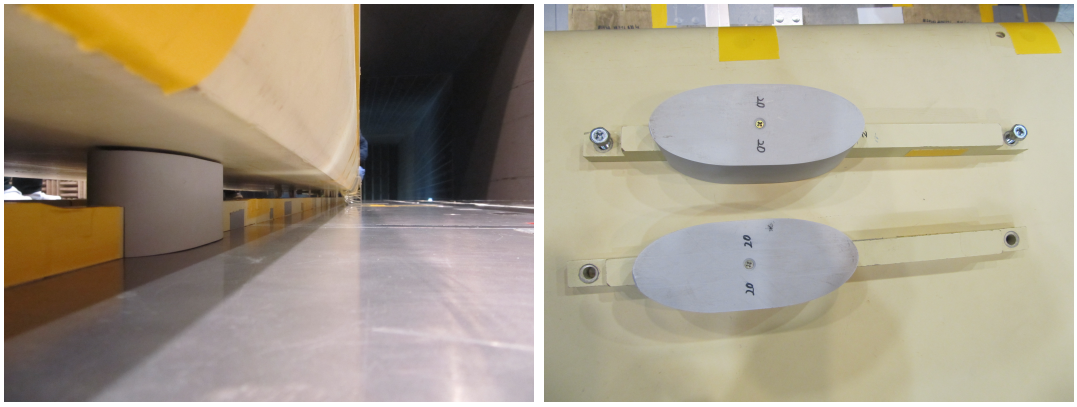

(a) (b)

Figure 11: Set-up used to achieve the leading car flow condition. (a) The width of the rail was increased attaching additional pieces. (b) View of the pieces used to increase the width of the rail.

Figure 13 shows the maximum, minimum and averaged values of one of the horizontal speed profiles obtained during the field tests at the rear bogie cavity inlet of the first and fifth cars of

(a) (b)

Figure 12: Set-up used to achieve the middle car flow condition. (a) The rails were not modified. (b) The ground plate was lowered to introduce an offset of 175 mm between the ground plate and the bottom edge of the nozzle.

the train for a height of -164.5 mm with respect to the train floor (which corresponds to -23.5mm in the case of the 1/7 scale train model). The speed profiles are compared with those obtained at the same position during the wind tunnel test for the leading and middle car configurations [2]. A good agreement is found between the wind tunnel and field tests flow speed profiles.

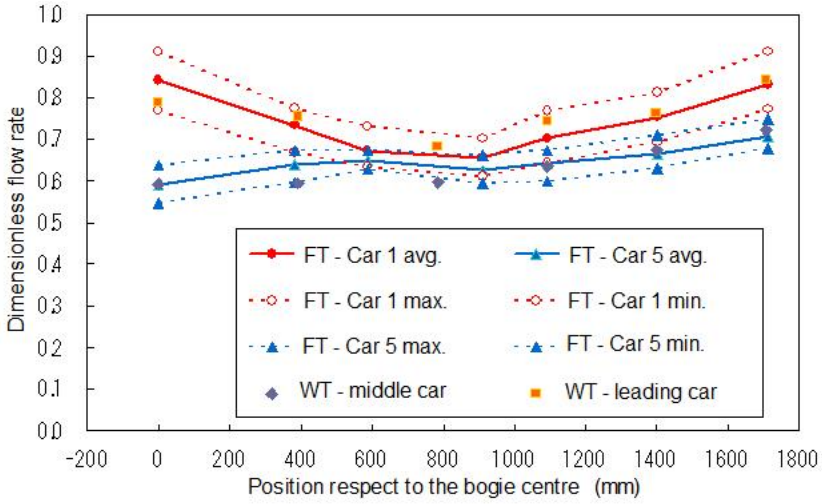

Figure 13: Horizontal flow speed profiles measured during the field tests (FT) at the inlet of the rear bogie cavity for the leading and fifth cars and speed profiles obtained during the wind tunnel tests (WT) for the leading and middle car configurations (for a distance of 23.5 mm with respect to the train floor).

2.5 Summary of the test configurations

The different experimental configurations that have been tested can be summarized as follows:

- Changes in the bogie cavity downstream edge: sharp and rounded edge.

- Changes in the interior components of the bogie mock-up: trailer bogie, motor bogie and side frames only.
- Evaluation of the noise from the side components by extending the wheel shafts by different lengths or using side covers.
- Changes in the flow speed profiles at the bogie cavity inlet: leading car and middle car flow configurations.

In order to make the presentation of the results easier, the nomenclature shown in Table 1 will be used throughout this report to name each of the test configurations.

Table 1: Summary of the configurations used during the wind tunnel tests and given case identifier.

Identifier	**Configuration**
Basic configurations: leading car flow configuration and cavity with rounded edges	
BG	Floor + skirts (Background noise)
C	Cavity with rounded edge
MB	Motor bogie
TB	Trailer bogie
FR	Just side frames
	Car position
+Mid	Middle car flow configuration
	Side noise
+S50	Side frame displaced laterally by 50 mm
+S75	Side frame displaced laterally by 75 mm
+S100	Side frame displaced laterally by 100 mm
	Other cases
+Sharp	Cavity with sharp edge
+Skirt	Full side skirts added

The acronyms shown in the table have the following meanings: BG (background noise), C (bogie cavity), MB (motor bogie), TB (trailer bogie) and FR (frames). These are used for the basic configurations, which were measured using the leading car flow configuration and the cavity with the rounded downstream edge. The identifier of the remaining cases tested is formed by adding the suffixes shown in Table 1 to the acronyms used for the standard configurations. As example, TB+Mid stands for the case with the trailer bogie and the middle car flow conditions and MB+S100 stands for the motor bogie with the wheel shaft extended by 100 mm.

3 Results and discussion

3.1 Analysis of the microphone array data

By applying a standard procedure the sound pressure level 2-D contour map is obtained. A grid of 20 by 20 values of Sound Pressure Level (SPL) covering an area around the bogie region (with spatial resolution of 0.1 m in both horizontal and vertical directions) was calculated for each of the frequency bands. The source position was localized by finding the cell of the grid containing the maximum SPL. Then, the values of the SPL were integrated in an area of 7 by 7 cells around the cell with the maximum value. This process was repeated for each of the frequency bands and bogie configurations. More details about the procedure followed to analyse the data from the microphone array is provided in the work published by Yamazaki et al [5].

The frequency resolution of the array limits the frequency range measured to values between 800 Hz and 20 kHz. This frequency range corresponds to the data measured using the 1/7 scale mock-up. In order to compare the results with the real case, the frequency range was converted to full scale by dividing the narrow band frequency vector by a factor of 7 and calculating afterwards the SPL for each of the equivalent 1/3 octave frequency bands. All the data measured with the microphone array is presented in full scale frequency range, with frequencies between 125 and 3,150 Hz. For the data measured by a single omnidirectional microphone the data is sometimes plotted against the 1/7 scale frequency range. In this case, a comment is included in each legend of the relevant figures. The amplitudes, however, are not scaled.

In order to calibrate the results obtained following the procedure described above the noise spectrum measured by an omnidirectional microphone for a reference case was compared with the noise spectrum calculated using the data from the microphone array. If the procedure followed to calculate the noise spectrum from the 2-D contour map is correct both noise spectra should agree. The differences between them are corrected by applying a frequency dependent conversion coefficient, which is calculated by subtracting both spectra for the reference case. Then, the conversion coefficient can be added to each of the frequency bands of the array noise spectra measured for the different test configurations [5].

The reference measurement was first made using a loudspeaker emitting broadband noise. It was found that for this case the noise spectrum measured by an omnidirectional microphone strongly depends on the position of the loudspeaker inside the bogie cavity and the orientation of the loudspeaker. For this reason, instead of using a loudspeaker as reference noise source it was preferred to use the bogie configuration MB+S100 that provides a good signal-to-noise ratio and it is more representative of the actual test conditions [5].

However, the position of the omnidirectional microphone used as reference microphone also influenced the results. Figure 14(a) shows the differences in the amplitude and spectral shape measured for the configuration MB+S100 and a flow speed of 320 km/h using different microphones of the array.

The position of each of the microphones of the array is shown in Figure 14(b). The noise spectrum from two adjacent microphones is very similar while the noise spectrum for microphones placed further away varies significantly. The reason for this disagreement still remains unknown but it may be the effect of the interference of the sound waves reflected on the ground surface.

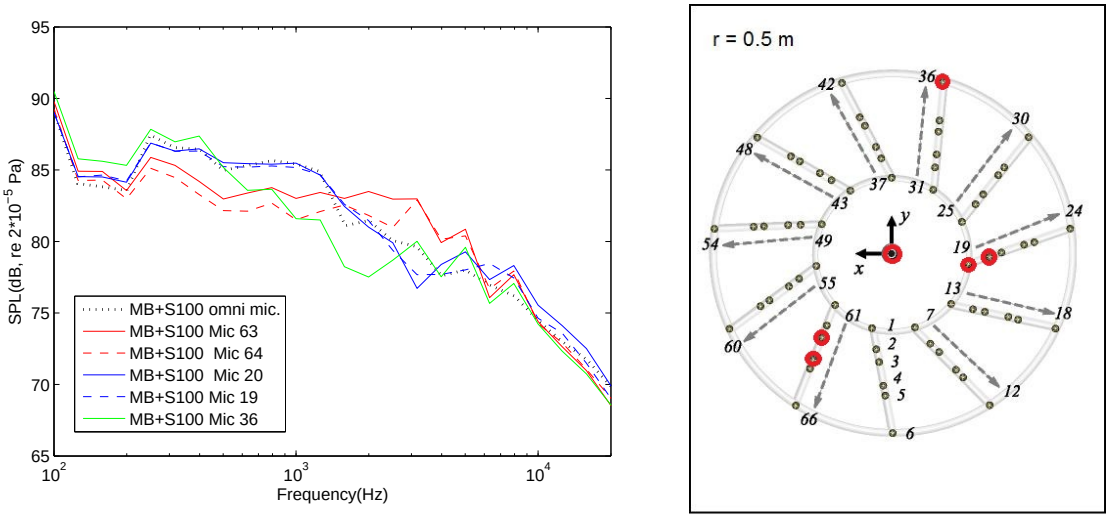

(a) (b)

Figure 14: (a) Noise spectra measured by different microphones during the tests with the configuration MB+S100 for a flow speed of 320 km/h. (b) Sketch showing the position of each of the microphones in the microphone array. The microphone called omni. mic. was located at the geometrical centre of the microphone array.

The omnidirectional microphone located at the centre of the microphone array was chosen as reference microphone used to obtain the conversion coefficient. Its location at the centre of the array minimizes the distance to other microphones in the array so the relative differences in the noise spectrum are less severe.

Figure 15 and Figure 16 show the noise maps for the configurations C and MB+S100 for different full scale 1/3 octave frequency bands. In all cases the noise source is located at the same place independently of the frequency band of analysis showing the broadband characteristic of the noise spectrum radiated by the bogie components. As expected, the resolution is quite poor for the frequency band of 250 Hz, improving as the frequency of analysis increases. The signal-to-noise ratio is high enough for all the frequency bands but it is less good in the frequency band of 1.6 kHz for the configuration C. Hereafter the noise maps for the 1/3 octave frequency band of 1 kHz will be shown as it is a good compromise between spatial resolution and signal-to-noise ratio.

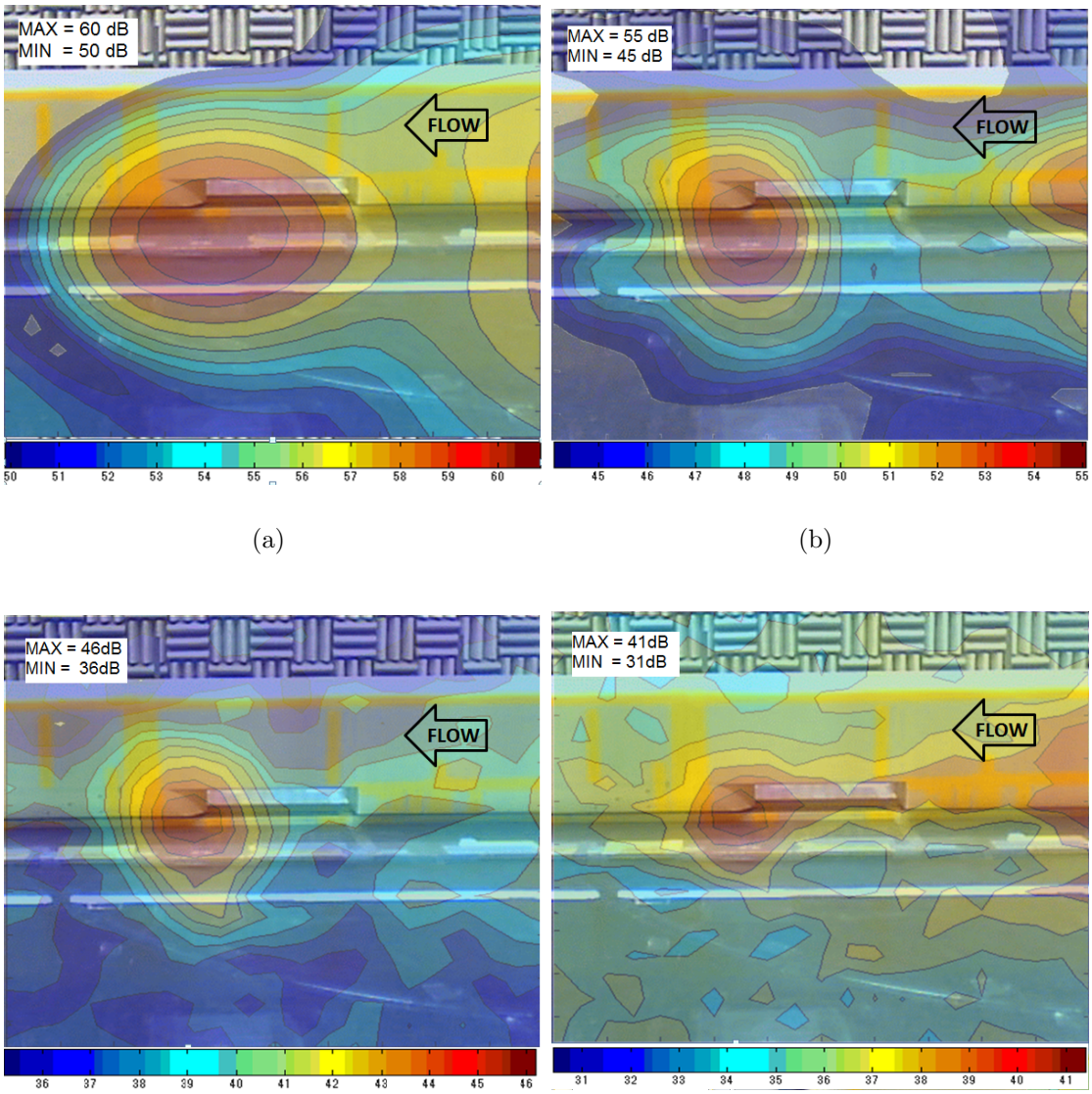

(a) (b)

(c) (d)

Figure 15: Noise maps for the configuration C for a flow speed of 320 km/h and full scale frequency range. (a) 1/3 octave frequency band of 250 Hz. (b) 1/3 octave frequency band of 500 Hz. (c) 1/3 octave frequency band of 1 kHz. (d) 1/3 octave frequency band of 1.6 kHz.

Figure 17 and Figure 18 show how the noise maps for the 1/3 octave frequency band of 1 kHz vary with the flow speed, for the cases MB and TB. If some of the noise sources (e.g. bogie cavity) scale with different speed exponents than the bogie components the noise maps might vary with the flow speed. Similarly, if the noise from the different bogie components have a different speed dependence the predominant noise source would change with the flow speed. The results shown in Figure 17 and Figure 18 do not show significant changes. Hereafter the noise maps will be presented for the flow speed of 320 km/h.

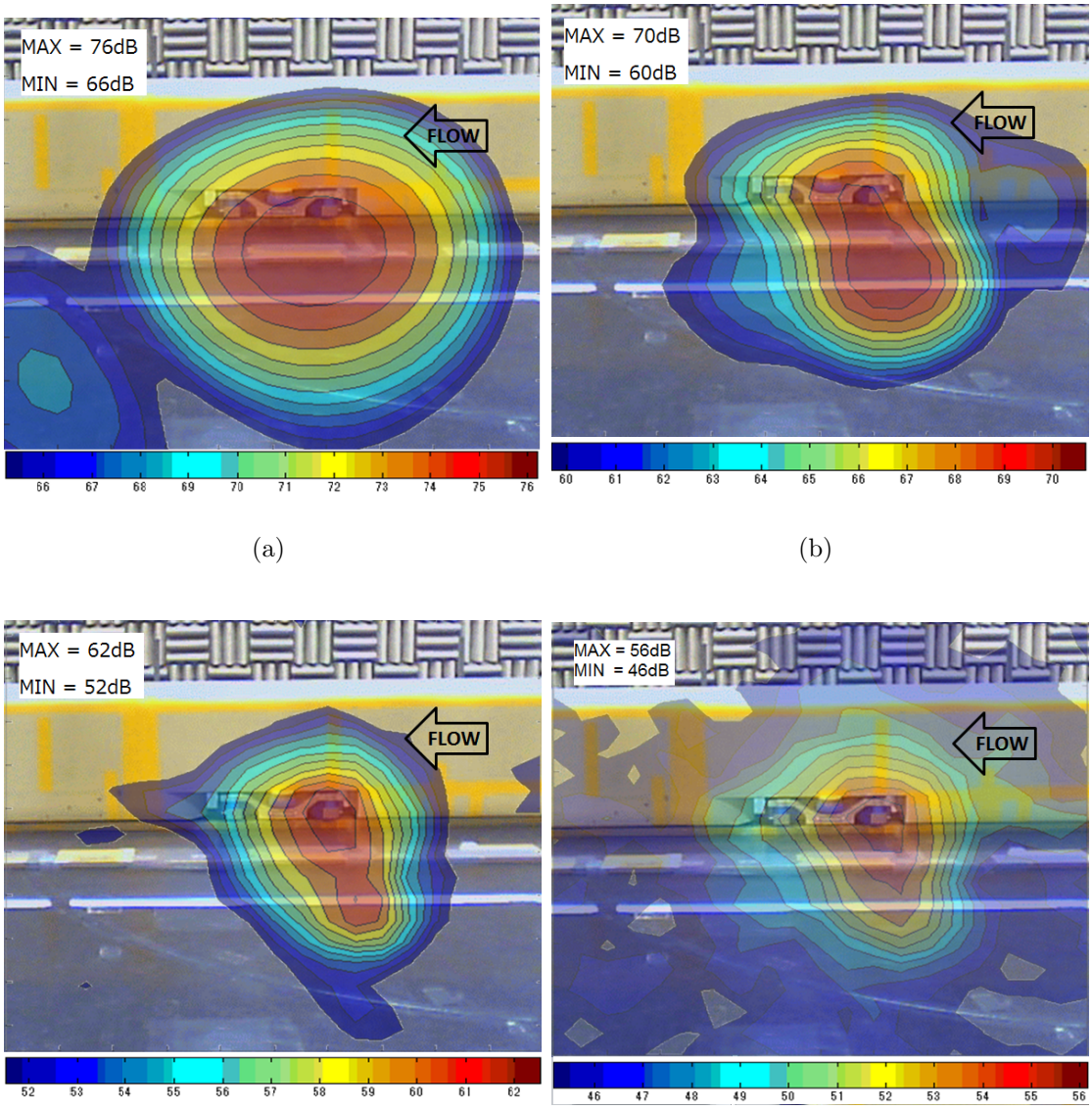

Figure 16: Noise maps for the configuration MB+S100 for a flow speed of 320 km/h and full scale frequency range. (a) 1/3 octave frequency band of 250 Hz. (b) 1/3 octave frequency band of 500 Hz. (c) 1/3 octave frequency band of 1 kHz. (d) 1/3 octave frequency band of 1.6 kHz.

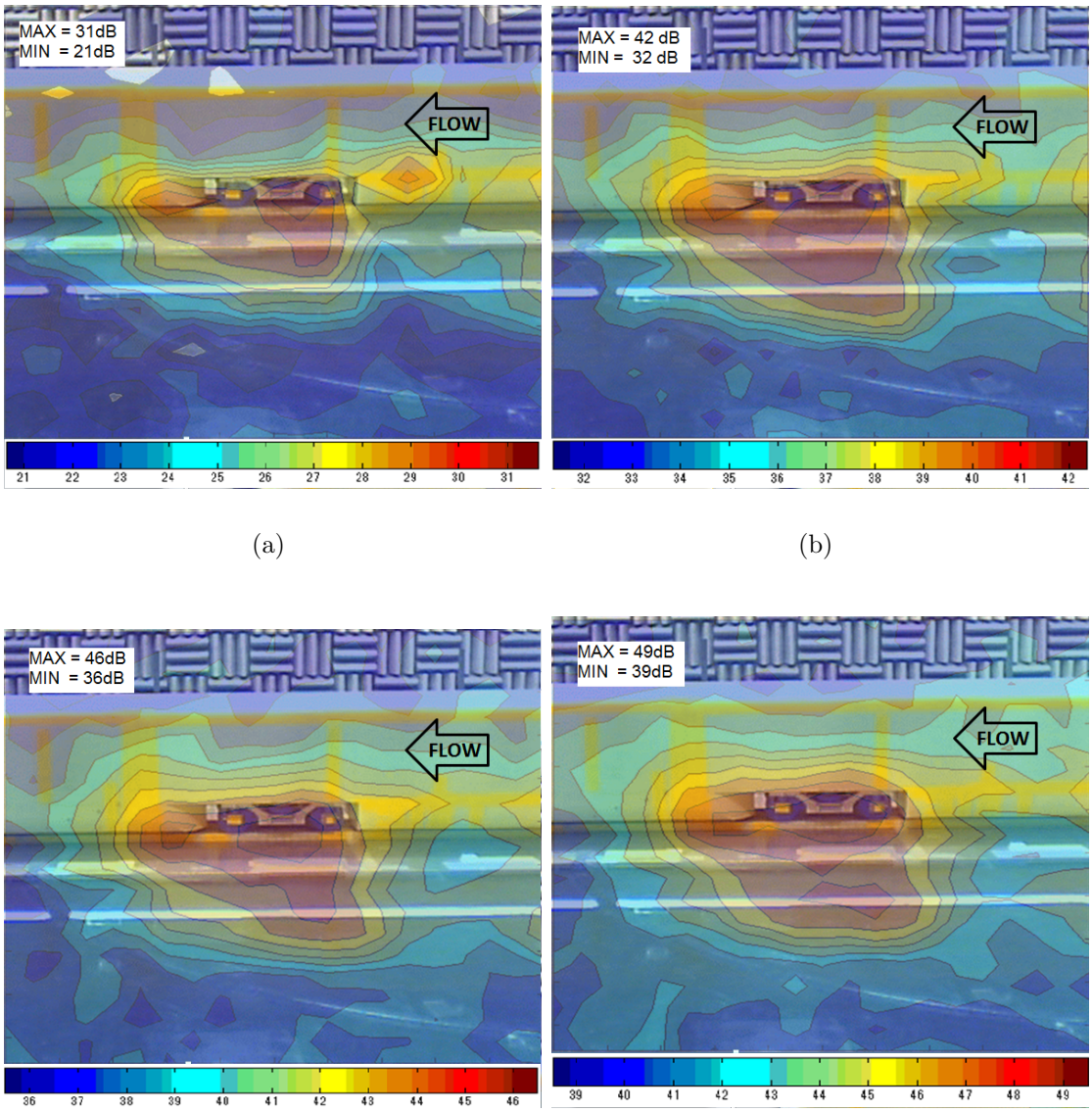

Figure 17: Noise maps for the configuration TB for the full scale 1/3 octave frequency band of 1 kHz. (a) flow speed of 180 km/h. (b) flow speed of 275 km/h. (c) flow speed of 320 km/h. (d) flow speed of 360 km/h.

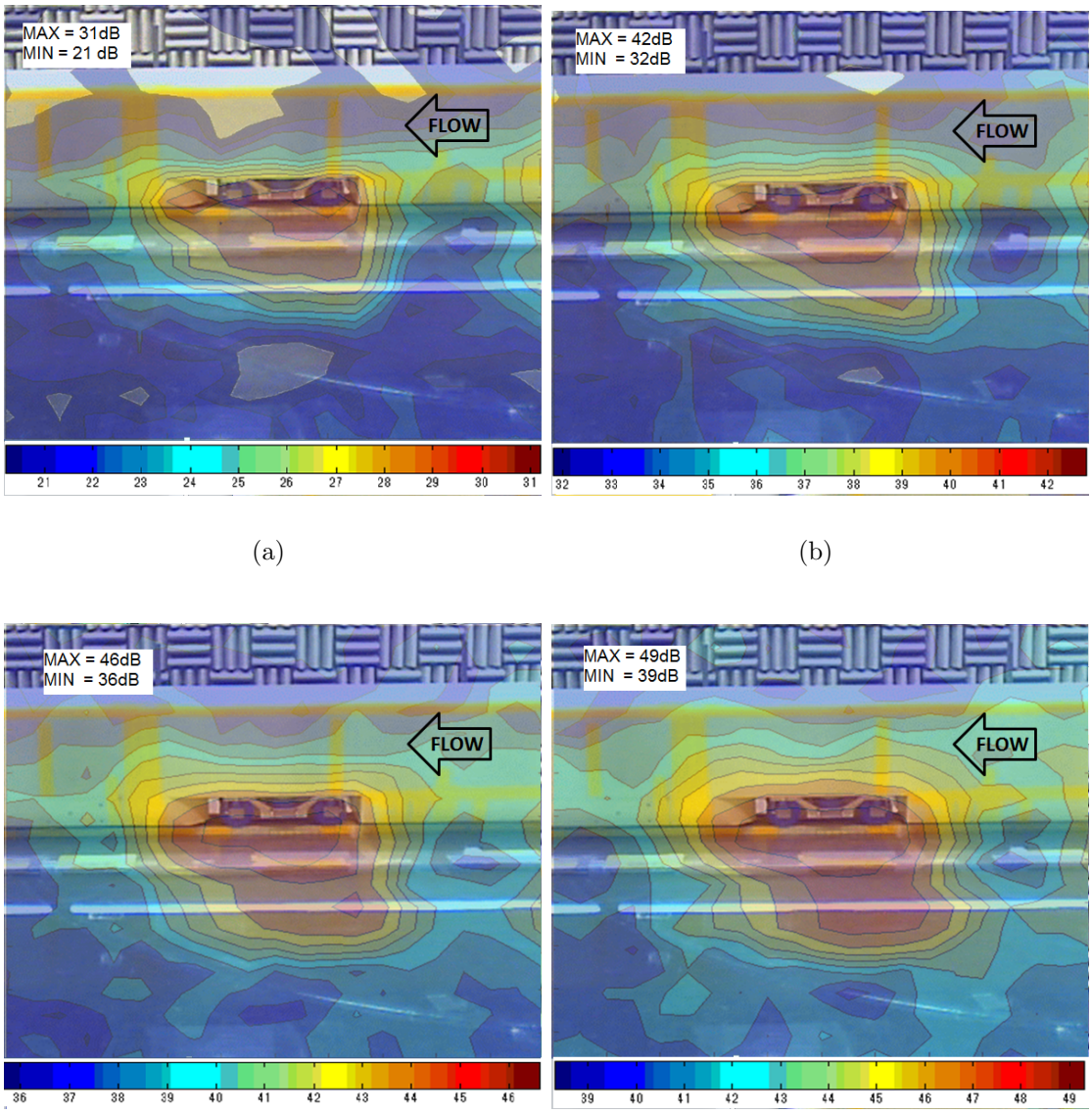

Figure 18: Noise maps for the configuration MB for the full scale 1/3 octave frequency band of 1 kHz. (a) flow speed of 180 km/h. (b) flow speed of 275 km/h. (c) flow speed of 320 km/h. (d) flow speed of 360 km/h.

3.2 Background noise and signal-to-noise ratio

The simplicity in the data analysis makes the use of an omnidirectional microphone, when possible, more convenient than the use of a microphone array. Nevertheless, the signal-to-noise ratio achieved using the omnidirectional microphone may be not high enough to assess the noise radiated by the bogie. Some analysis is included next on the signal-to-noise ratio obtained using the omnidirectional microphone placed at the centre of the microphone array for the different test configurations.

Figure 19 shows the comparison between the noise spectrum from the configurations MB and MB+S100 measured in two different tests carried out during two different days. Differences in the

Overall Sound Pressure Level (OSPL) lower than 1 dB were obtained, showing a good repeatability of the results. The results are presented in the frequency range as measured.

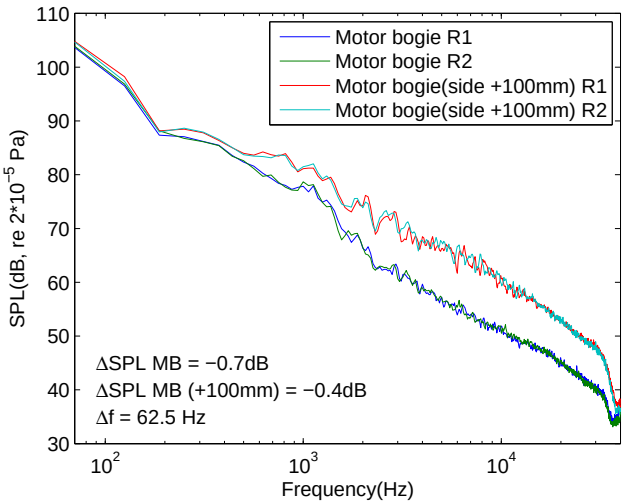

Figure 19: Noise spectrum radiated by the configurations MB and MB+S100 measured in two different test rounds carried out during two different days. Flow speed of 320 km/h and frequency range as measured.

The configuration BG (shown in Figure 20) is taken as background noise since it includes the noise generated by noise sources other than those located in the bogie cavity region. Figure 21 provides a good indication of the signal-to-noise ratio obtained using the omnidirectional microphone. The interest of including the results from the configurations C and C+Sharp (shown in Figure 3) in Figure 21 is two-fold. If the noise generated by the configuration BG is subtracted from the noise generated by the configuration C+Sharp then the noise generated by the cavity itself is obtained. This noise can be taken as the effective background noise as the main interest is to assess the noise produced by the bogie itself. If the noise from the configurations C+Sharp and C are compared, the effect of rounding the downstream edge of the cavity can be evaluated.

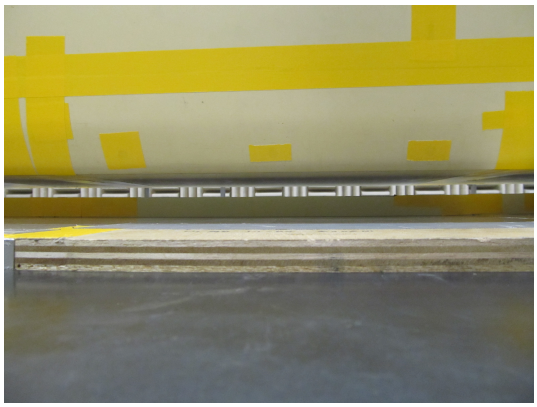

Figure 20: To assess the background noise the bogie cavity was covered using side skirts and extending the train floor (BG configuration).

According to the results shown in Figure 21 the signal-to-noise ratio for the configurations MB, C and C+Sharp is not enough (lower than 3 dB in most of the 1/3 octave bands) when compared with the configuration BG. The noise spectra for these cases have to be obtained from the measurements made by using the microphone array. Same evaluation was made for the cases MB+Mid, TB+Mid

and C+Mid with respect to the case BG+Mid. Nevertheless, the signal-to-noise ratio obtained for the configuration MB+S100 is high enough showing its feasibility to be used for the directivity measurements. It can be also stressed that the wind tunnel background noise is predominant for 1/3 octave bands below 200 Hz, for the frequency range as measured.

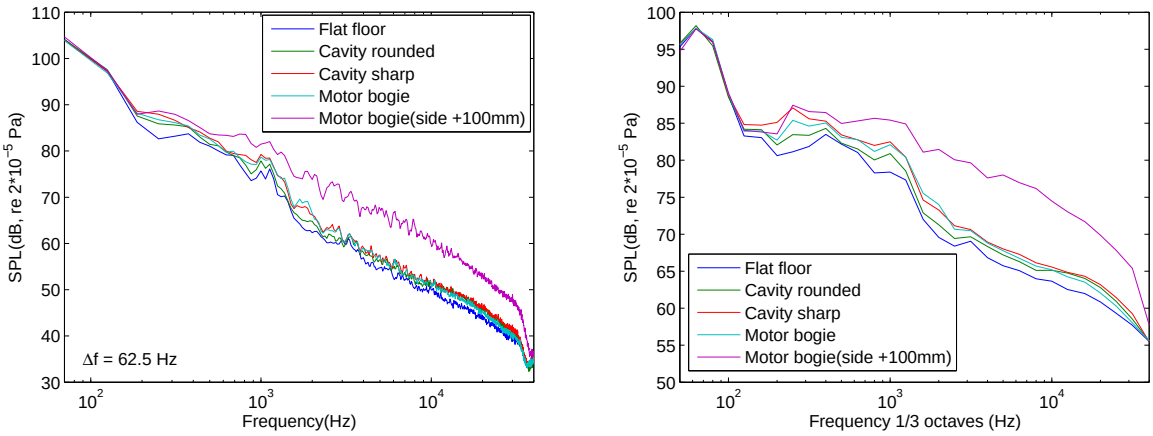

(a) (b)

Figure 21: Noise spectra acquired by the omnidirectional microphone using the configurations BG, C, MB, MB+S100 and C+Sharp for a flow speed of 320 km/h and a frequency range as measured. (a) Spectrum in narrow band (b) Spectrum in 1/3 octaves.

Figure 22 shows a significant improvement of the signal-to-noise ratio obtained for the configurations MB and MB+Mid using the integrated noise spectra obtained from the microphone array. Nevertheless, the background noise increases at high frequencies, reducing the signal-to-noise ratio in this frequency range. The cause of the high-frequency noise was not identified and it can be defined as the noise floor related to the experimental set-up.

The noise from the configuration C was subtracted from the noise spectrum of the different configurations. For these cases the suffix C was added to the configuration identifier, as shown in Figure 23. The 1/3 octave bands of the corrected data for which the signal-to-noise ratio was lower than 3 dB are highlighted using triangular markers. For the configurations MB+S100 and MB+S75 the cavity noise (configuration C) is negligible. The configuration MB+S50 is barely affected by the cavity noise except at high frequencies. However, the configuration MB is highly affected by the noise from the cavity and, in most of the 1/3 octave frequency bands, the signal-to-noise ratio was lower than 3 dB, making it impossible to obtain reliable results when applying the background noise correction. Hereafter, no background noise correction was applied to the data unless otherwise stated. These results and subsequent ones are shown in the full scale frequency range.

3.3 Cavity noise

Figure 24 shows the effect of rounding the downstream edge of the bogie cavity as measured by the microphone array. The reduction in the noise spectrum amplitude is between 3 and 7 dB depending on the 1/3 octave frequency band. For high frequencies the reduction is smaller due to

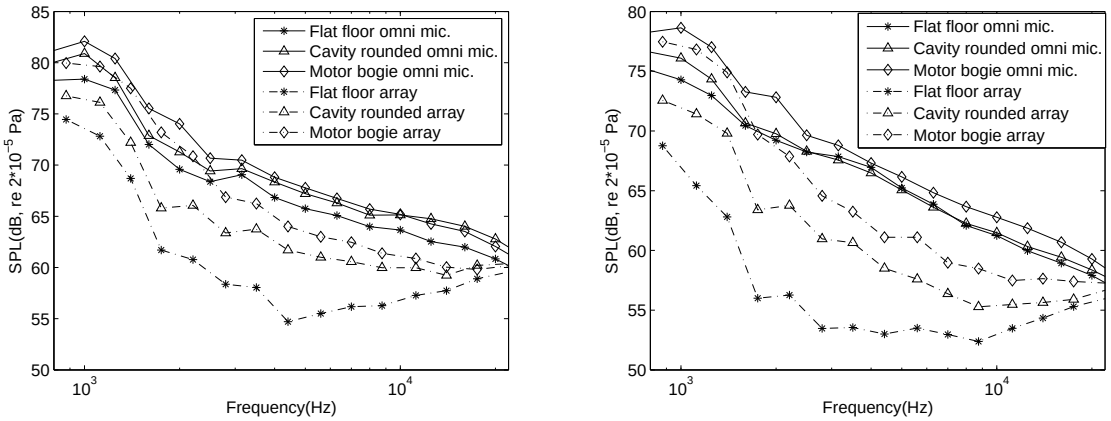

(a) (b)

Figure 22: Comparison between the noise radiated by the motor bogie and the background noise measured using the omnidirectional microphone and using the integrated noise spectra from the microphone array. Flow speed of 320 km/h and frequency range as measured. (a) Leading car flow configuration. (b) Middle car flow configuration.

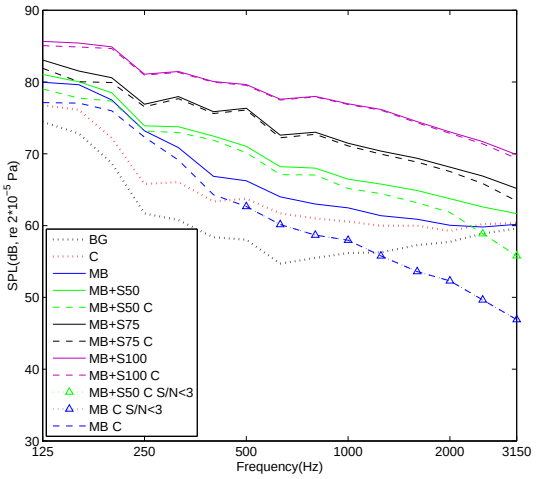

Figure 23: Noise spectra obtained for the different motor bogie side noise configurations before and after subtracting the cavity noise. Leading car flow configuration, flow speed of 320 km/h and full scale frequency range. The 1/3 octave bands for which the signal-to-noise ratio was lower than 3 dB are highlighted using triangular markers.

the influence of the background noise. A reduction of 3.7 dB in the OSPL was obtained. It should be pointed out that the noise spectrum from the trailer bogie is masked by the noise radiated by the cavity with the sharp edge. The effect of rounding the downstream edge of the cavity seems crucial in order to obtain a high enough signal-to-noise ratio.

Figure 25 shows the noise maps for the configurations C and C+Sharp. In both cases the predominant noise source is localized at the downstream edge of the bogie cavity. The noise radiated by the sharp edge is 4 dB higher that the noise produced by the rounded version.

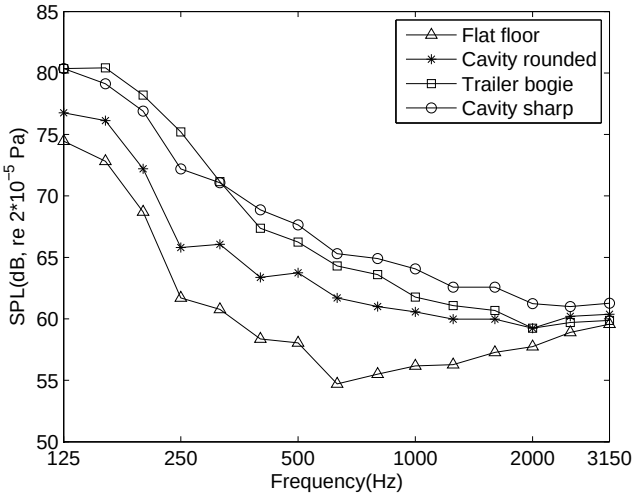

Figure 24: Effect of rounded the downstream edge of the bogie cavity. Integrated noise spectra using the data from the microphone array for the leading flow configuration, a flow speed of 320 km/h and full scale frequency range.

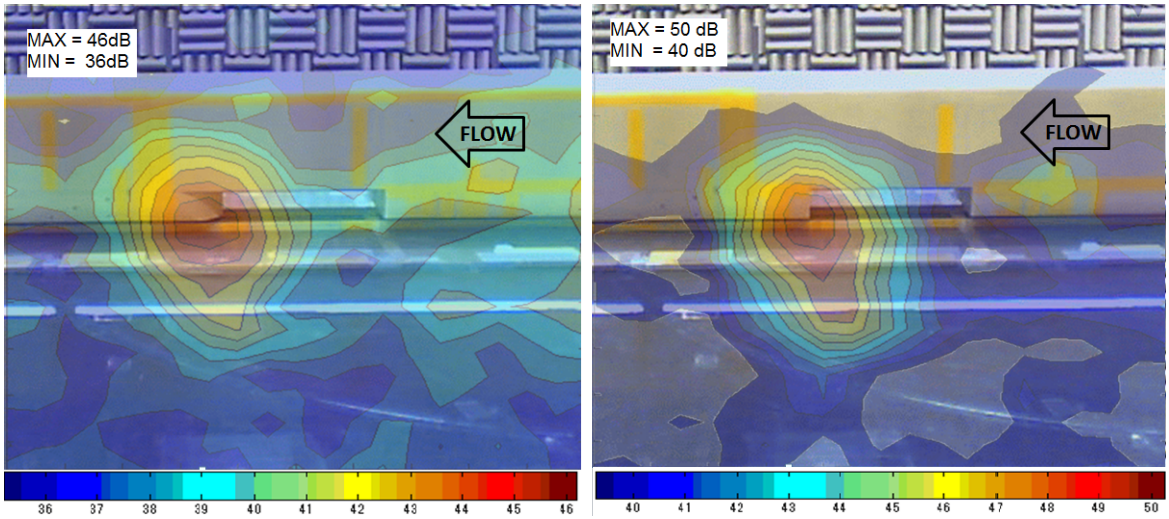

(a) (b)

Figure 25: Noise map for the full scale 1/3 octave frequency band of 1kHz. Flow speed of 320 km/h . (a) Cavity with a rounded downstream edge. (b) Cavity with a sharp downstream edge.

3.4 Internal component noise

The noise from the configurations MB, TB and FB (details of these bogie configurations are shown in Figure 4) is compared in Figure 26, allowing the influence of the internal components on the noise radiation to be assessed. The noise spectra from the trailer and motor bogie are quite similar, with differences smaller than 2 dB in the whole frequency range. When the internal components (including wheels) are removed the noise decreases significantly and the amplitude of the noise spectrum becomes very close to that radiated by the bogie cavity.

Figure 27 shows how the noise is localized in the bogie region for both the motor and the trailer

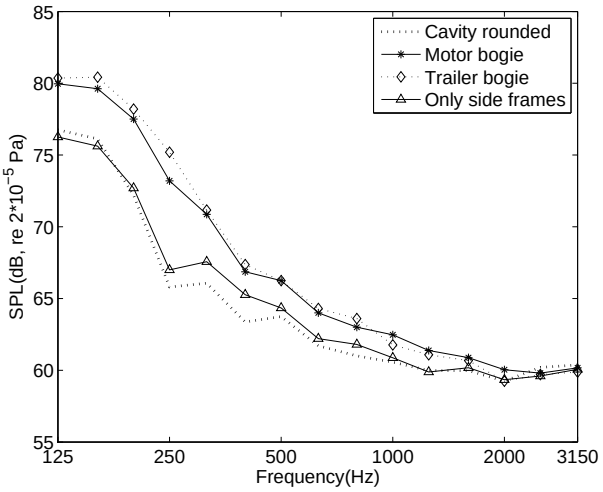

Figure 26: Comparison between the noise radiated by the motor and trailer bogie configurations and the noise radiated by just the side frames. Leading car flow configuration, flow speed of 320 km/h and full scale frequency range.

bogie but it is not possible to detect a specific noise source inside it. In the case of the trailer bogie a noise spot is located at the downstream edge of the cavity.

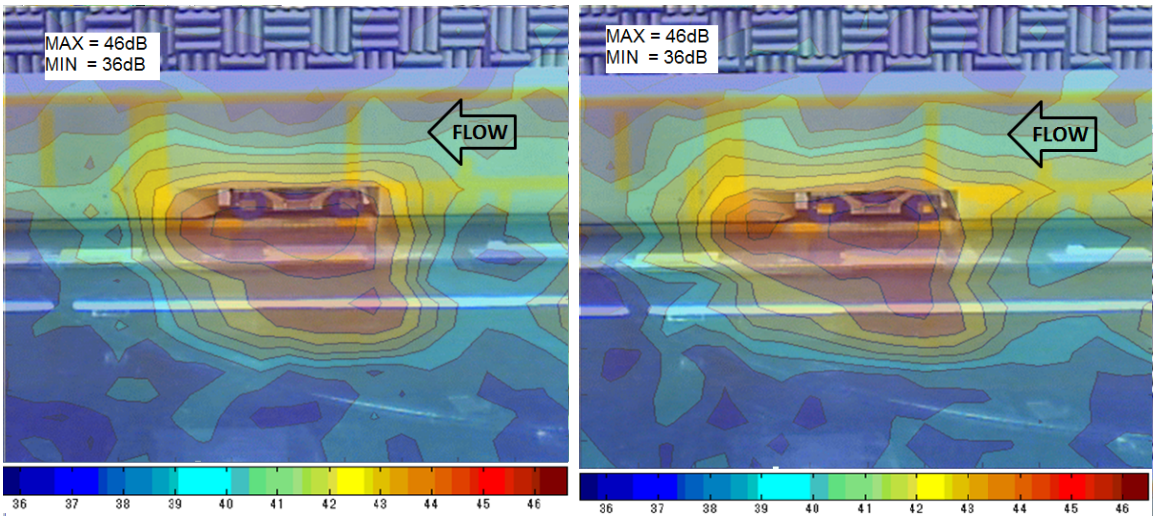

(a) (b)

Figure 27: Noise map for the full scale 1/3 octave frequency band of 1kHz. Flow speed of 320 km/h. (a) Motor bogie (MB). (b) Trailer bogie (TB).

Looking at the noise map for the frequency band of 1 kHz it is not possible to see any difference between the maximum SPL radiated by the motor bogie and the trailer bogie. The OSPL radiated by the motor bogie is in this case 84.8 dB while the OSPL radiated by the trailer bogie is 85.5 dB. This difference is quite small so it is difficult to draw conclusions from these data. Nevertheless, the slightly higher OSPL for the trailer bogie case could be due to the increase of the surface area of the components that are not shielded by the upstream step of the bogie cavity. Figure 28 shows a sketch of the front view of the bogie cavity area where the bogie components, or parts of them, which are exposed to the incoming flow can be identified. The wheels are the components

with most surface area exposed to the incident flow but these components are included in both the motor and trailer bogie. The difference between the two configurations is in the internal components. The surface area of the brake disks that is not shielded by the cavity is larger than the corresponding surface area of the motor and gear box. This may be the reason why the noise from the trailer bogie is around 1 dB higher than the noise from the motor bogie.

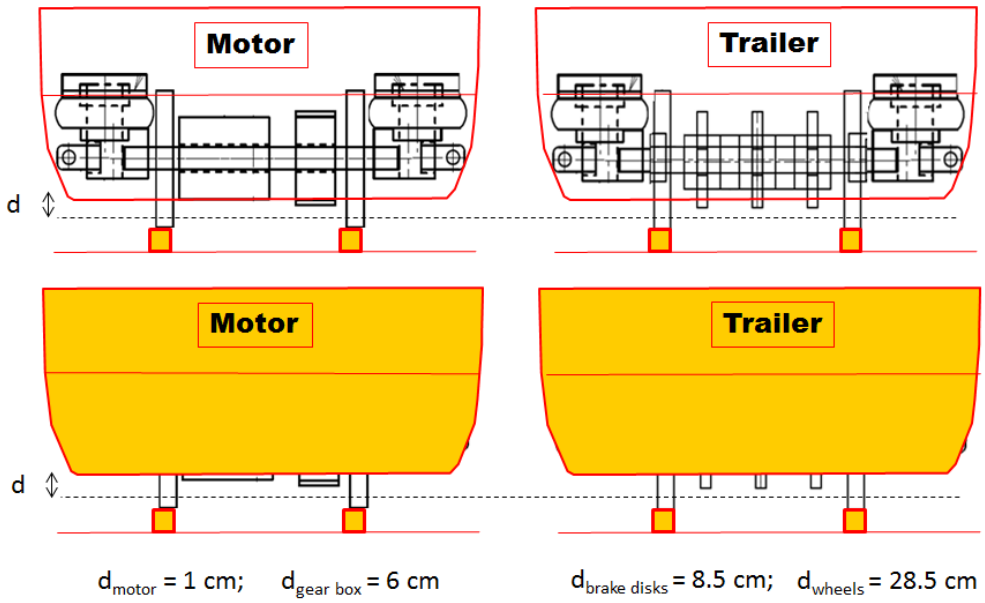

Figure 28: Sketch showing the frontal view of the MB and TB configurations. In the sketches on the top all the components are visible while in the sketches on the bottom only the parts of components which are not shielded by the bogie cavity are visible.

Figure 29 shows the effect of partially shielding the side noise using full side covers (configuration MB+Skirt, as shown in Figure 4). The inclusion of the side covers reduces the noise by about 2 or 3 dB in most of the 1/3 octave frequency bands except for the high frequencies, for which the background noise is significant. This noise reduction may be due to the shielding of the noise radiated by the interior components and also because the side skirt prevents the lateral flow from impinging on the side components and the downstream edge of the cavity.

When the full side skirt is attached the predominant noise source cannot be localized precisely and the noise is seen just to come out from the bogie cavity through the gap between the ground and the side skirts, as shown in Figure 30(a). In the case of having just the side frames inside the cavity, shown in Figure 30(b), the main source of noise is the cavity downstream edge showing that no significant contribution is coming from the side frames.

3.5 Effect of the flow configuration

Figure 31 shows the grid of positions where the mean flow speed was measured using the rake of Pitot tubes. The measurement plane was located at the inlet of the bogie cavity. The position of the measurement points can be associated with the position of the bogie components allowing assessment of the incident flow speed for each of them.

Following the coordinates shown in Figure 31 the horizontal and vertical flow speed profiles for

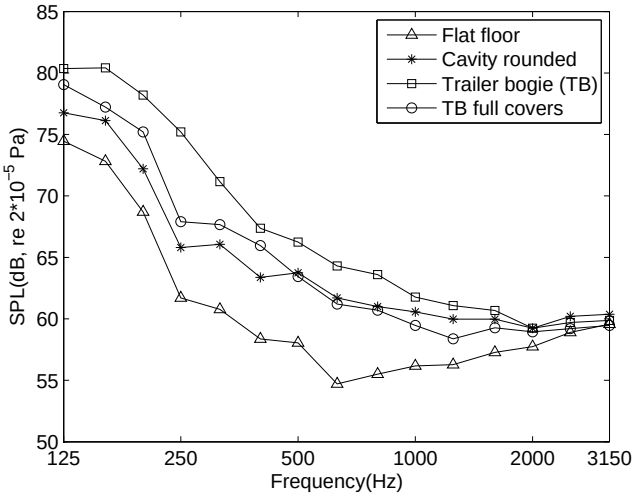

Figure 29: Effect of the bogie full side covers on the noise radiated by the trailer bogie. Leading car flow configuration, flow speed of 320 km/h and full scale frequency range.

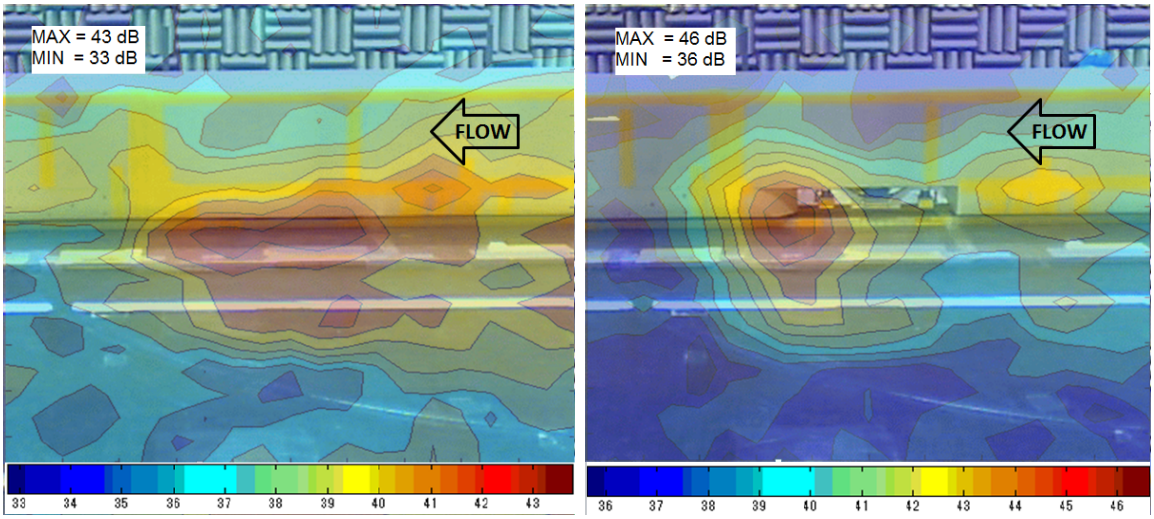

(a) (b)

Figure 30: Noise map for the full scale 1/3 octave frequency band of 1 kHz. Flow speed of 320 km/h. (a) Motor bogie with full side covers (MB+Skirt). (b) Only frames (FR).

the leading car flow configuration are shown in Figure 32.The results for the middle car are shown in Figure 33. Contour maps are shown in Figure 34.

Some conclusions can be drawn from the results for the leading car flow configuration:

- The lowest flow speeds are at the points close to the surfaces (ground and car floor). The sudden change in the flow speed for the distance of 244 mm and a normalized height of 0.02 shows how this effect disappears when the measurement point is out of the bogie cavity.
- The flow speed is slightly lower at the positions above the rail, i.e. 112 mm from the centre (incident flow speed for the wheels).

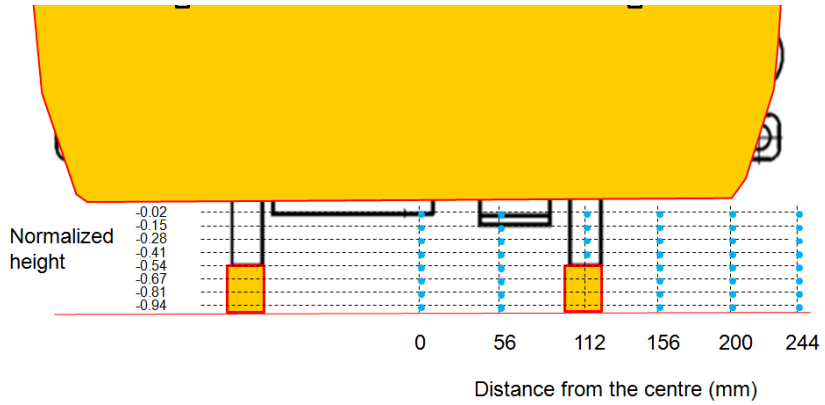

Figure 31: Sketch showing the positions of the bogie cavity inlet where the mean flow speed was measured.

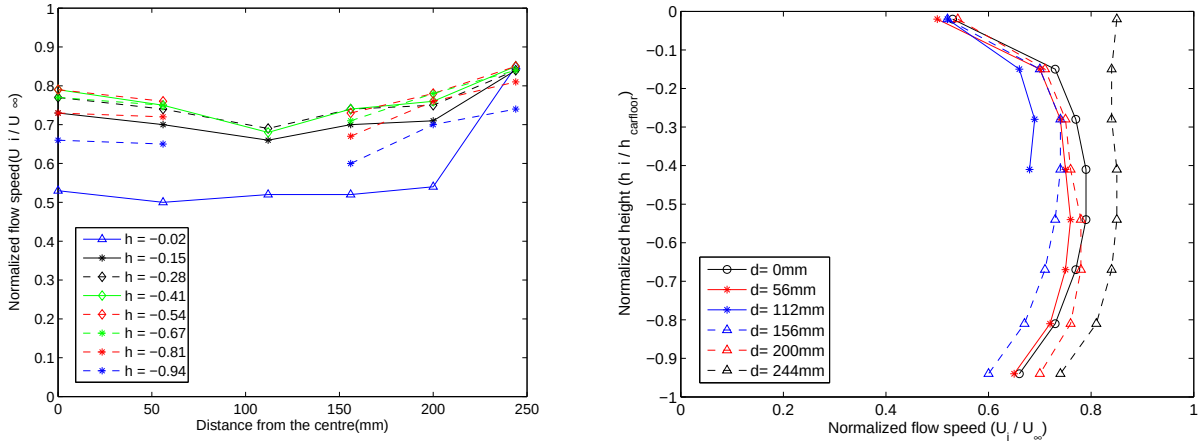

(a) (b)

Figure 32: Flow speed profiles at the bogie cavity inlet for the leading car flow configuration. (a) Horizontal profile. (b) Vertical profile.

- The flow speed is higher at the positions outside the bogie cavity, i.e. above 200 mm.

The following conclusions are inferred from the results for the middle car flow configuration:

- The same reduction in the flow speed is detected close to the surfaces.
- The flow speed is quite constant for positions between the rails, gradually increasing for positions beyond the rails.
- The flow speeds in the area between the rails are lower than those for the leading car flow configuration, having values very close to those measured in front of the wheel.

These conclusions can also be observed in the contour maps shown in Figure 34.

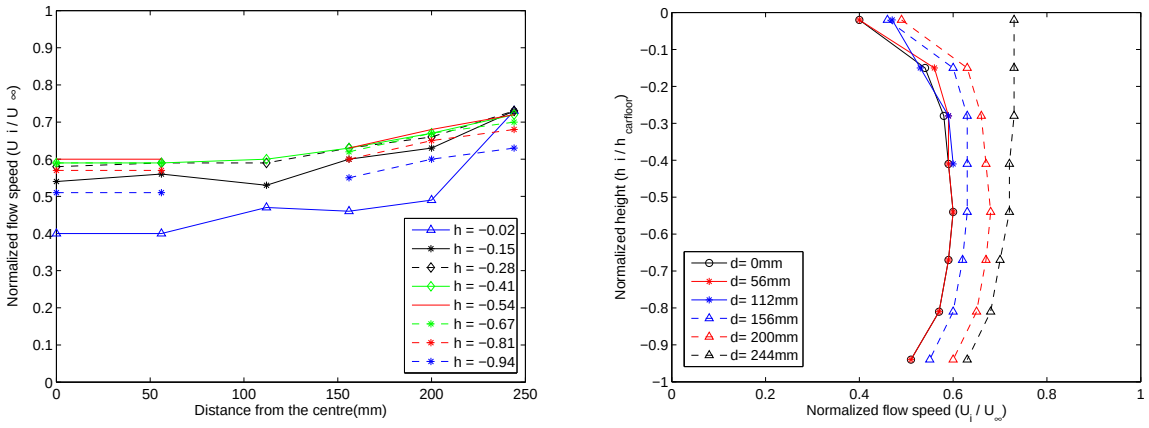

(a) (b)

Figure 33: Flow speed profiles at the bogie cavity inlet for the middle car configuration. (a) Horizontal profile. (b) Vertical profile.

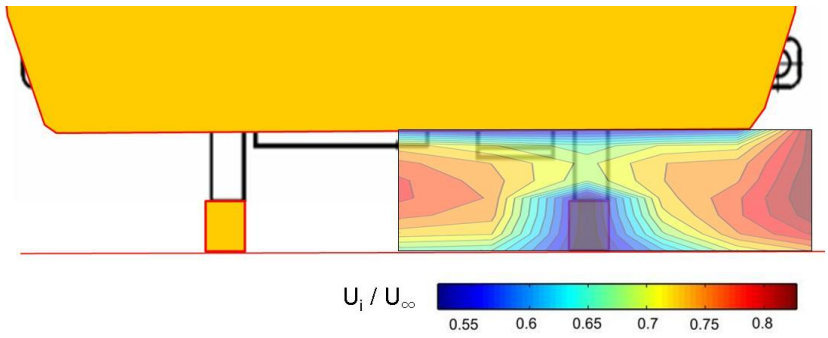

(a)

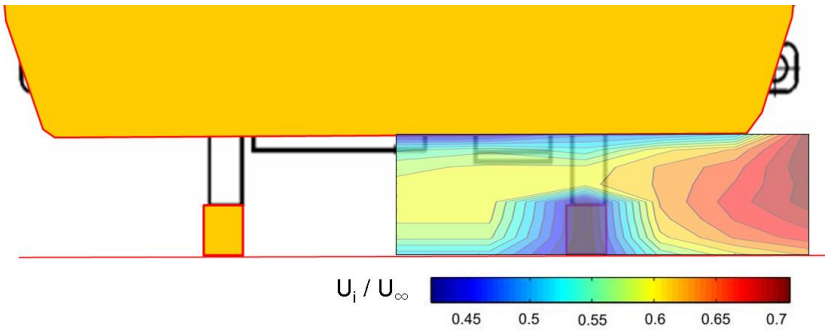

(b)

Figure 34: Contour map showing the normalized flow speed at the bogie cavity inlet. (a) Leading car flow configuration. (b) Middle car flow configuration.

Figure 35 (a) shows the noise spectra radiated by the motor bogie, the trailer bogie and the cavity for the leading car and the middle car flow configurations. Figure 35 (b) shows the difference between the SPL radiated by each of the bogie configurations if the leading car and the middle

car flow conditions are compared.

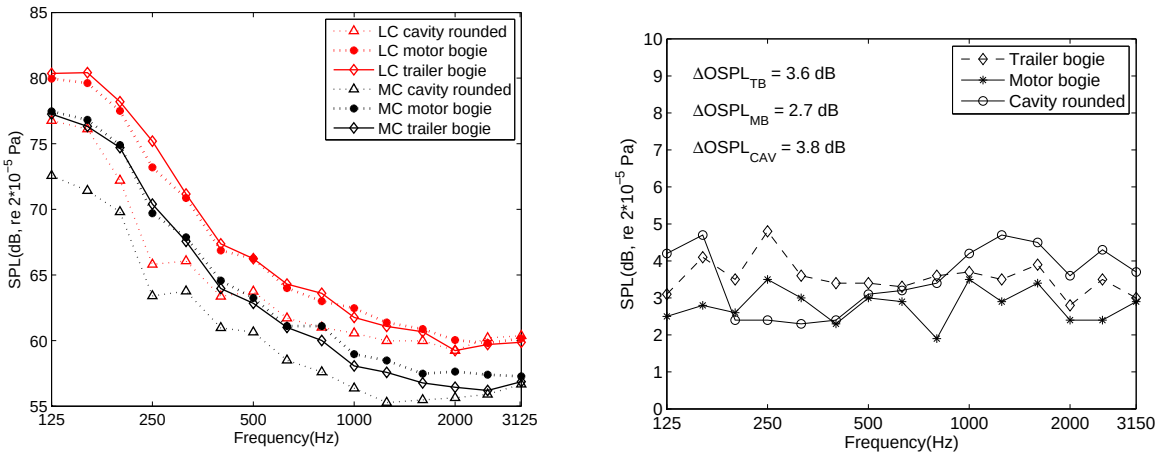

(a) (b)

Figure 35: Motor bogie, trailer bogie and cavity noise for the leading car and middle car flow configuration. Flow speed of 320 km/h and full scale frequency range. (a) Noise spectra. (b) OSPL differences.

The noise spectra are higher for the cases tested with the leading car flow configuration, as expected due to the higher incident flow speed. In terms of overall SPL, ΔSPL is very similar for the configurations TB and C (3.6 and 3.8 dB) and is around 1 dB lower for the configuration MB. The values of ΔSPL are quite constant over the whole frequency range for all the bogie configurations, with a variability less than 2 dB.

For comparison Figure 36 shows the ratio $U_{middle}/U_{leading}$, where U_{middle} and $U_{leading}$ are the mean flow speeds measured at the different positions of the cavity inlet where the Pitot tubes were located, for the middle car and leading car flow configurations. The colour map shows that the highest differences in the flow speed are located in the area between the rails. The variation of the incident flow speed is higher in the positions where the internal components are.

The legend included in Figure 36 also shows the expected reduction in the noise radiated by a bogie component exposed to the incoming flow if the middle car flow conditions are compared with the leading car flow conditions. The theoretical factor $10 \times log_{10}(U)^{\alpha}$ was used for the calculations. A value of α equal to 6.5 was used (see the section 3.7 for more details). For example, the ratio $U_{middle}/U_{leading}$ varies along the surface of the wheel but, if it is approximated to an average value of 0.85, this leads to a difference of -4.2 dB in the OSPL radiated by the wheels between the middle and the leading car flow conditions.

3.6 Bogie side noise

Figure 37 shows the upper and frontal views of the bogie side when installed in the bogie cavity after extending the axles by different lengths. When the axles were not extended (motor bogie as it is) no bogie components protrude out of the side of the cavity but, with the shaft extension, it can be seen how some of the components or parts of the components are not shielded anymore by

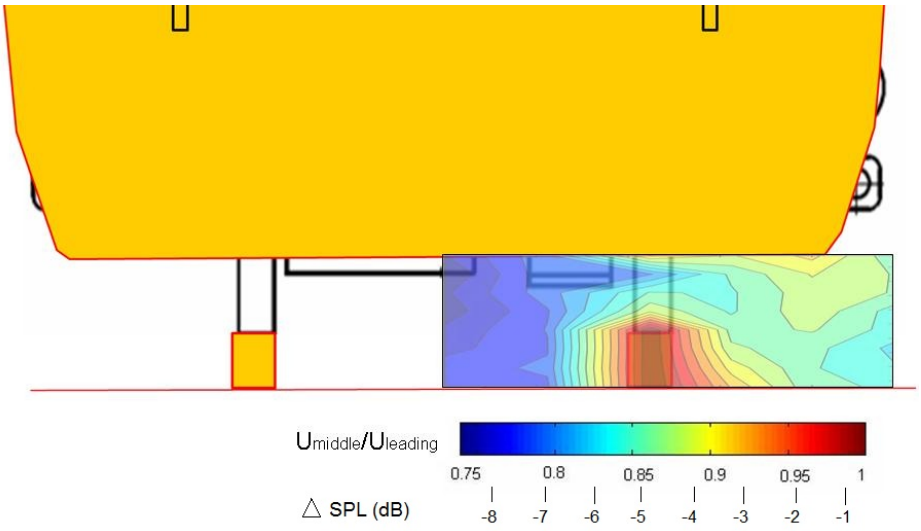

Figure 36: Colour map showing the ratio $U_{middle}/U_{leading}$ for each of the areas where the Pitot tubes were placed.

the bogie cavity. This fact will lead to an increase in the incident flow speed impinging on those components.

The purpose of the sketches included in Figure 38 is to show in more detail which components or parts of components are outside the bogie cavity for each of the shaft extension lengths and in which proportion. This can be used to assess the surface area of each component exposed to the side flow, so a simplistic prediction of the increase in the noise radiation with the position of the bogie components outside the cavity can be assessed by using the theoretical factor $10\times\log_{10}(\Delta S)$, where $\Delta S = S_i/S_{ref}$ and S_i is the surface area exposed to the side flow of the ith- side noise configuration, e.g. S_{75} for the configuration MB+S75, and S_{ref} is the surface area taken as reference, in this case S_{50} that is the surface area exposed to the side flow for the bogie configuration MB+S50.

The noise spectrum increases the for each of the shaft extensions, as shown in Figure 39. Even if the noise increases in all the frequency bands this is lower at low frequencies. For this reason, instead of looking at the increase of the overall SPL, the average increase along the frequency bands was assessed.

Table 2 shows the average increase in the SPL over the 1/3 octave frequency bands obtained when the configurations with the wheel shafts extended by different lengths are compared with the standard motor bogie configuration, for each of the flow speeds. For a shaft extension of 50 mm the lateral damper is the only component that is exposed to the side flow leading to an average increase of the SPL over the 1/3 octave bands between 3.1 and 3.3 dB, depending on the flow speed. When the shaft extension increases, a higher number of the bogie components are placed outside the bogie cavity and consequently the noise increases. However, the increase in the SPL seems to be independent of the flow speed.

Figure 40 a), Figure 40 c) and Figure 40 e) shows that when ΔSPL is plotted against the Strouhal number for the cases described above the results do not collapse well. This is a consequence of the fact that ΔSPL is nearly independent of the flow speed when plotted against frequency, as shown in Figure 40 b), Figure 40 d) and Figure 40 f).

The variation of the SPL obtained when the bogie shafts are extended by different lengths with

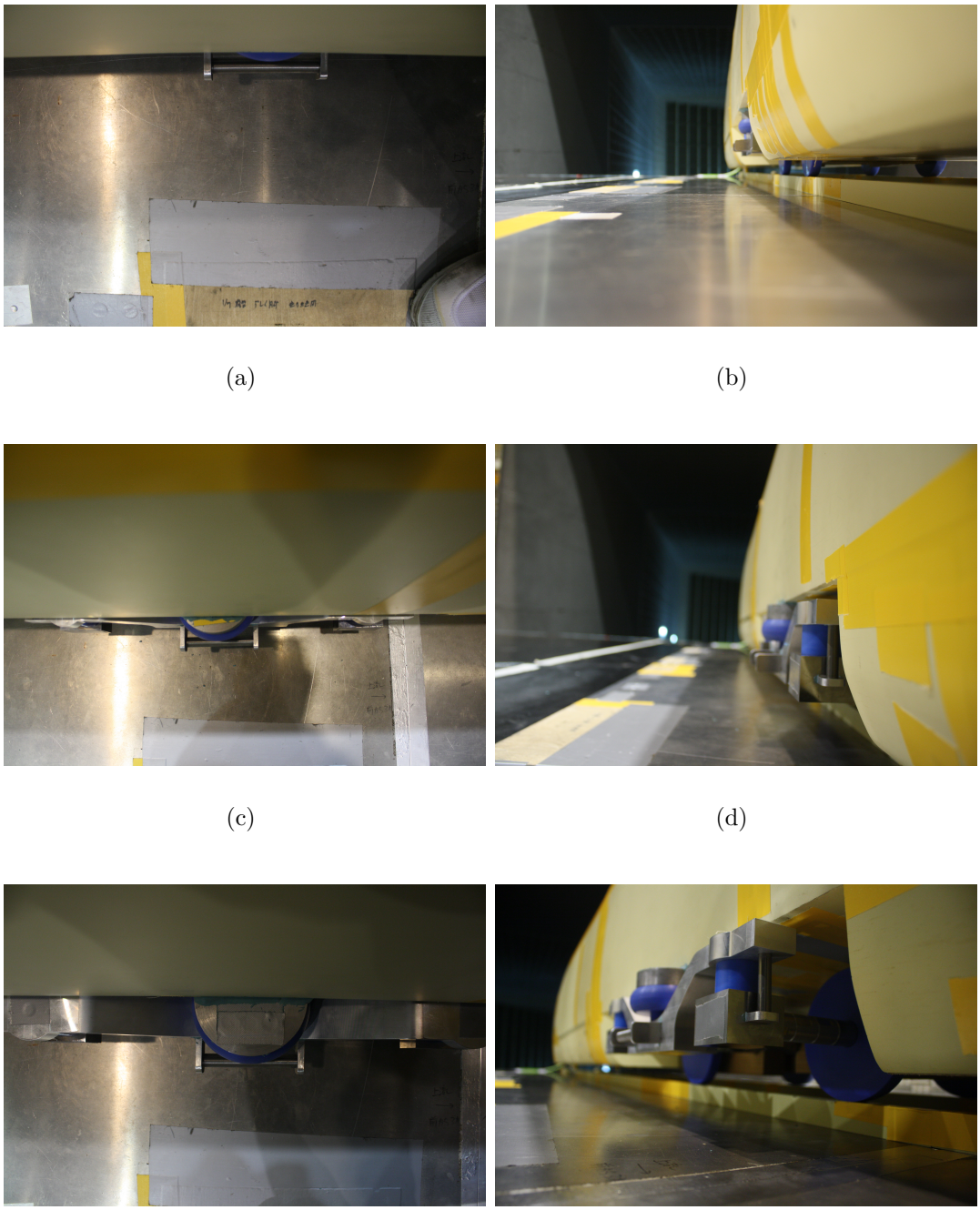

(a) (b)

(c) (d)

(e) (f)

Figure 37: Bogie mounted in the cavity for the side noise measurements. (a) Side displacement of 50 mm. Upper view. (b) Side displacement of 50 mm. Frontal view. (c) Side displacement of 75 mm. Upper view. (d) Side displacement of 75 mm. Frontal view. (e) Side displacement of 100 mm. Upper view. (f) Side displacement of 100 mm. Frontal view.

respect to the standard bogie case for each of the flow speeds are plotted against frequency, as shown in Figure 41. ΔSPL increases significantly for mid- and high-frequencies but the difference is lower in the low-frequency range. This fact can be explained by the influence of the low-frequency background noise in the measurements with the configuration MB. Therefore in the following this configuration will be omitted.

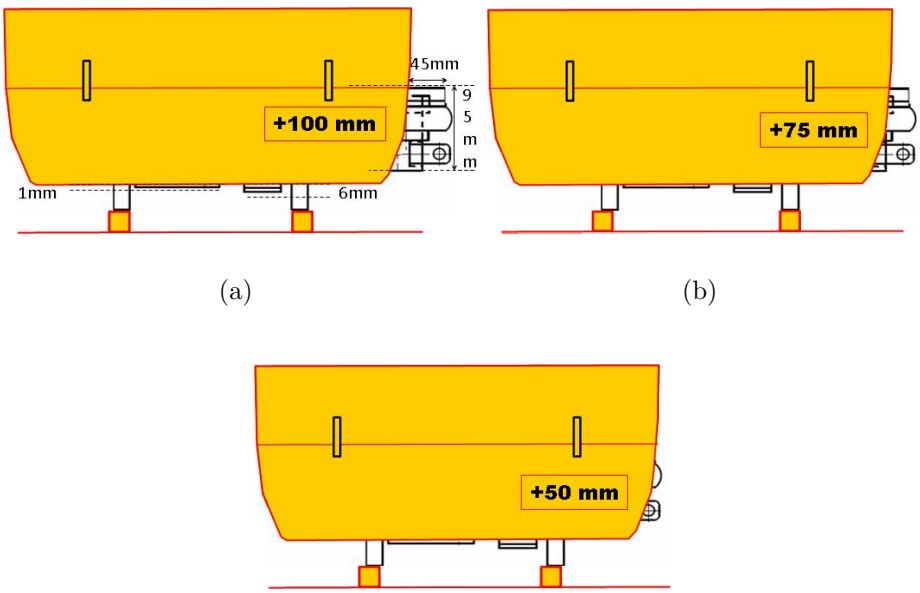

(a) (b)

(c)

Figure 38: Sketch showing the relative position of the bogie components respect to the car body for the different shaft extensions (frontal view). (a) Side displacement of 100 mm. (b) Side displacement of 75 mm. (c) Side displacement of 50 mm.

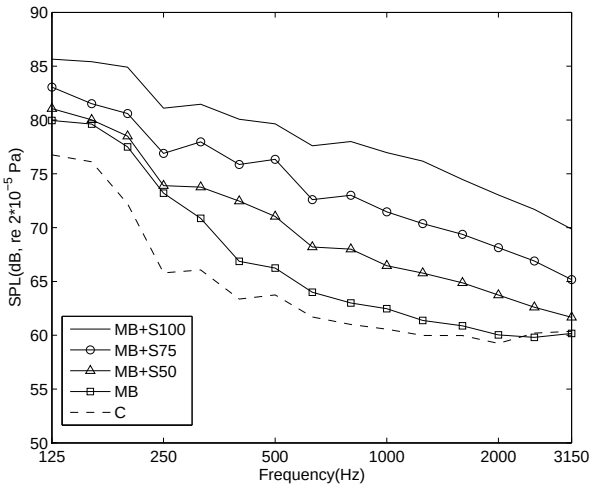

Figure 39: Noise spectrum radiated by the different bogie side noise configurations. Flow speed of 320 km/h and full scale frequency range.

The comparison between the different configurations with the wheel shafts extended allows an assessment to be made of the influence of the increment of the surface area of the bogie components exposed to the side flow. Table 3 shows the average ΔSPL over the 1/3 octave bands when the configurations MB+S50, MB+S75 and MB+S100 are compared with each other. When the side frame extension length is increased then the surface area of the components exposed to the side flow also increases. The increase in the SPL in this case can be roughly calculated applying the factor $10 \times log_{10}(\Delta S)$, where ΔS is the ratio of the surface areas exposed to the side flow and the factor $10 \times log_{10}(\Delta U)^{\alpha}$, where ΔU is the ratio of the speeds of the flow impinging the surface of the bogie side components and α is the speed exponent. At a sufficient lateral distance from the

Table 2: Average SPL difference over the 1/3 octave bands between the standard motor bogie configuration MB and the extended axle configurations MB+50, MB+S75 and MB+S100 for different flow speeds.

	ΔSPL (dB, re 2×10^{-5} Pa)		
Flow speed (km/h)	ΔSPL_{+S50}	ΔSPL_{+S75}	ΔSPL_{+S100}
180	3.1	7.4	11.9
275	3.3	7.0	11.5
320	3.1	6.9	11.3
360	3.3	6.9	11.2

car body the flow speed is expected to be the same as the mainstream flow velocity. However, close to the car body surface the flow speed will be lower. The flow speed profiles at the side of the car body have been not measured but, looking at the results shown in Figure 34, it can be seen how for the positions more distant from the bogie centre, which lie outside the bogie cavity, the flow speeds are still not equal to the mainstream flow speed.

Table 3: Average increase of the SPL over the 1/3 octave bands (ΔSPL) when the configurations MB+S100, MB+S75 and MB+S50 are compared with each other for the different flow speeds.

	ΔSPL (dB, re 2×10^{-5} Pa)		
Flow speed (km/h)	$\Delta SPL_{MB+S75/MB+S50}$	$\Delta SPL_{MB+S100/MB+S75}$	$\Delta SPL_{MB+S100/MB+S50}$
180	4.4	4.4	8.8
275	3.7	4.5	8.2
320	3.8	4.5	8.3
360	3.5	4.2	7.9
average	3.9	4.4	8.3
$\Delta SPL_{Theoretical}$	2.5 ($\Delta S = 1.78$)	2.7 ($\Delta S = 1.86$)	5.2 ($\Delta S = 3.31$)

The theoretical factor included in Table 3 only accounts for the increase in the surface area exposed to the side flow. It can be seen how the theoretical value underestimates the change in the OSPL between two different side configurations, and this difference is higher for bigger changes of the surface area. This disagreement can be explained as the velocity impinging on the side components is not uniform in the horizontal direction and for larger distances to the bogie centre the local flow speed becomes closer to the mainstream flow speed.

Figure 42 shows how ΔSPL varies with the Strouhal number and the frequency for the cases included in Table 3. ΔSPL appears to be nearly independent of the flow speed for both cases, when plotted against the Strouhal number and the frequency.

Figure 43 shows ΔSPL to be nearly constant when plotted against frequency with maximum differences of 2-3 dB for each of the flow speeds. It can then be inferred that the differences in ΔSPL between the low frequencies and the mid and high frequencies shown in Figure 41 are due to the influence of the background noise in the measurements with the configuration MB.

Figure 44 shows the noise maps of the 1/3 octave frequency band of 1 kHz for the configurations MB, MB+S50, MB+S75 and MB+S100. For the configuration MB the noise source is located around the bogie region but it is not possible to pinpoint a specific component as the most significant noise source. When the wheel shafts are extended by 50 mm (configuration MB+S50)

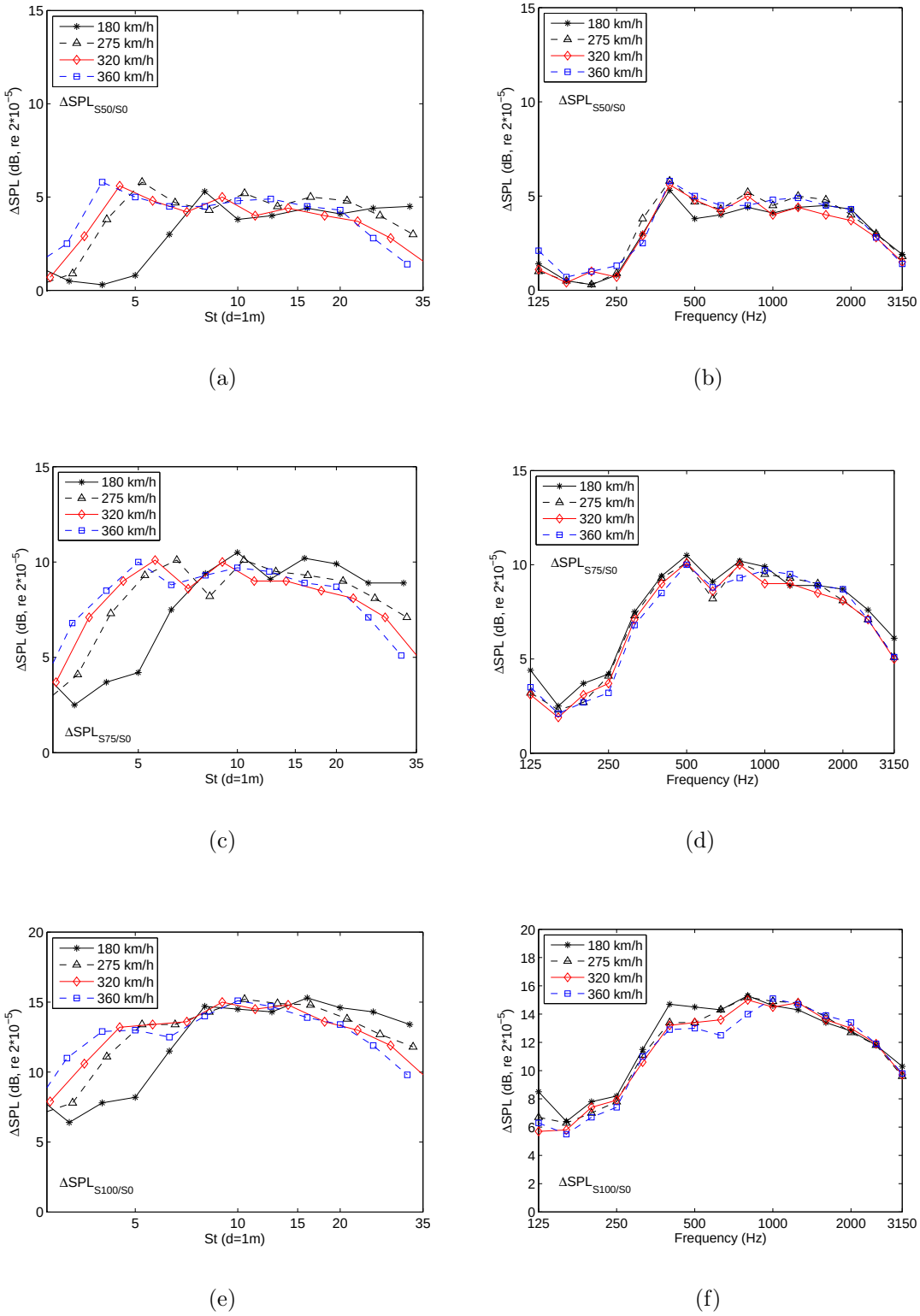

Figure 40: ΔSPL as a function of the Strouhal number and the frequency for the comparison between the cases MB+S50 ($\Delta SPL_{S50/S0}$), MB+S75 ($\Delta SPL_{S75/S0}$) and MB+S100 ($\Delta SPL_{S100/S0}$) and the case MB. (a) $\Delta SPL_{S50/S0}$ vs. Strouhal number. (b) $\Delta SPL_{S50/S0}$ vs. frequency. (c) $\Delta SPL_{S75/S0}$ vs. Strouhal number. (d) $\Delta SPL_{S75/S0}$ vs. frequency. (e) $\Delta SPL_{S100/S0}$ vs. Strouhal number. (f) $\Delta SPL_{S100/S0}$ vs. frequency.

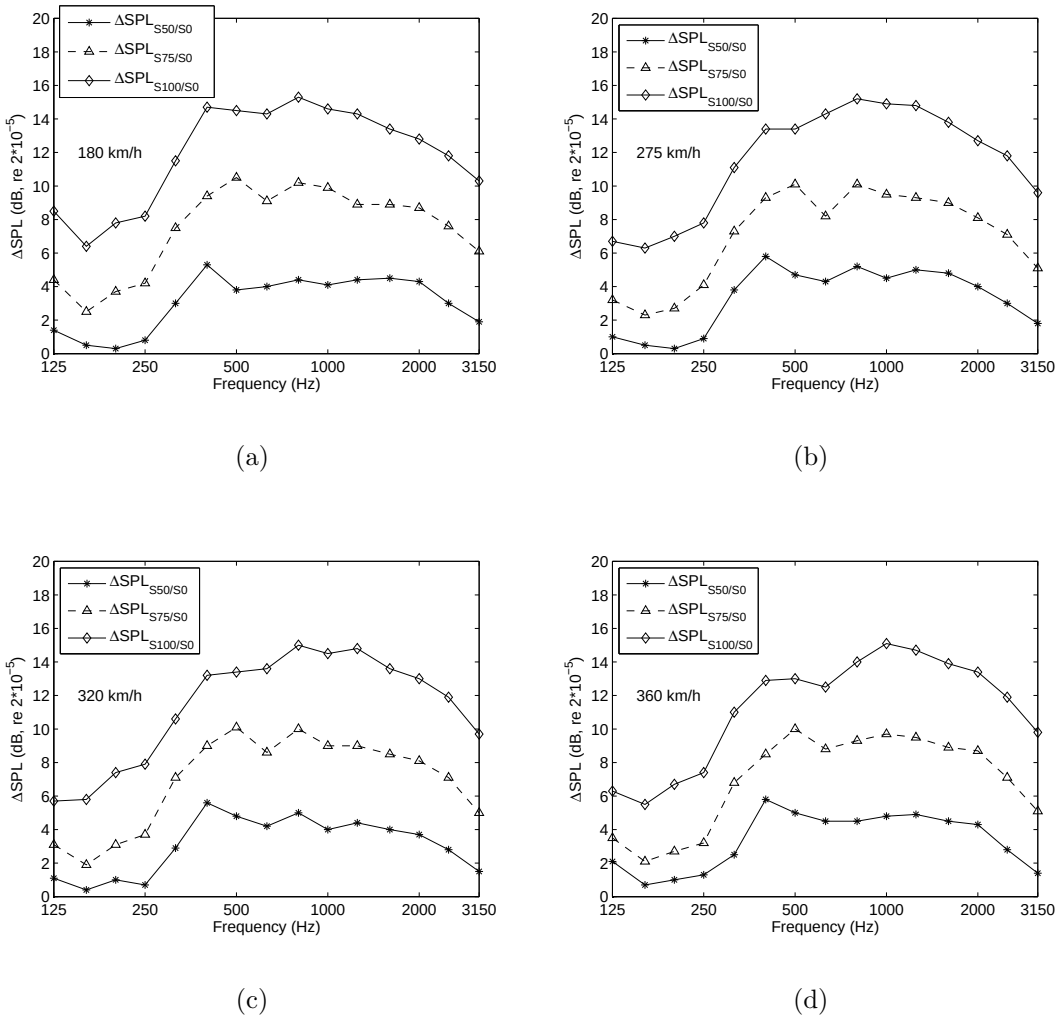

(a) (b)

(c) (d)

Figure 41: ΔSPL as a function of the frequency when the surface area of the components outside the bogie cavity increases due to the increment of the shaft extension length. The configuration MB is taken as reference.

the lateral damper is found to be the main noise source. With a shaft extension of 75 mm equal contribution is found for the lateral damper and the front of the side frame, while the latter is the dominant noise source for a shaft extension of 100 mm. These results show the importance of the side components when they are exposed to the side flow.

3.7 Speed exponent

The speed exponent α was calculated as the slope of the OSPL when plotted against the flow speed after applying linear curve fitting. The same procedure was followed to calculate the speed exponent for each frequency band from the slope obtained from the increment with the flow speed of the SPL for each frequency band.

The speed exponents obtained for the configurations MB, MB+S50, MB+S75 and MB+S100 are shown in Figure 45(a). The frequency range used was between 160 Hz and 3,150 Hz (full scale) and the background noise correction was applied to the data. Despite some variability present in

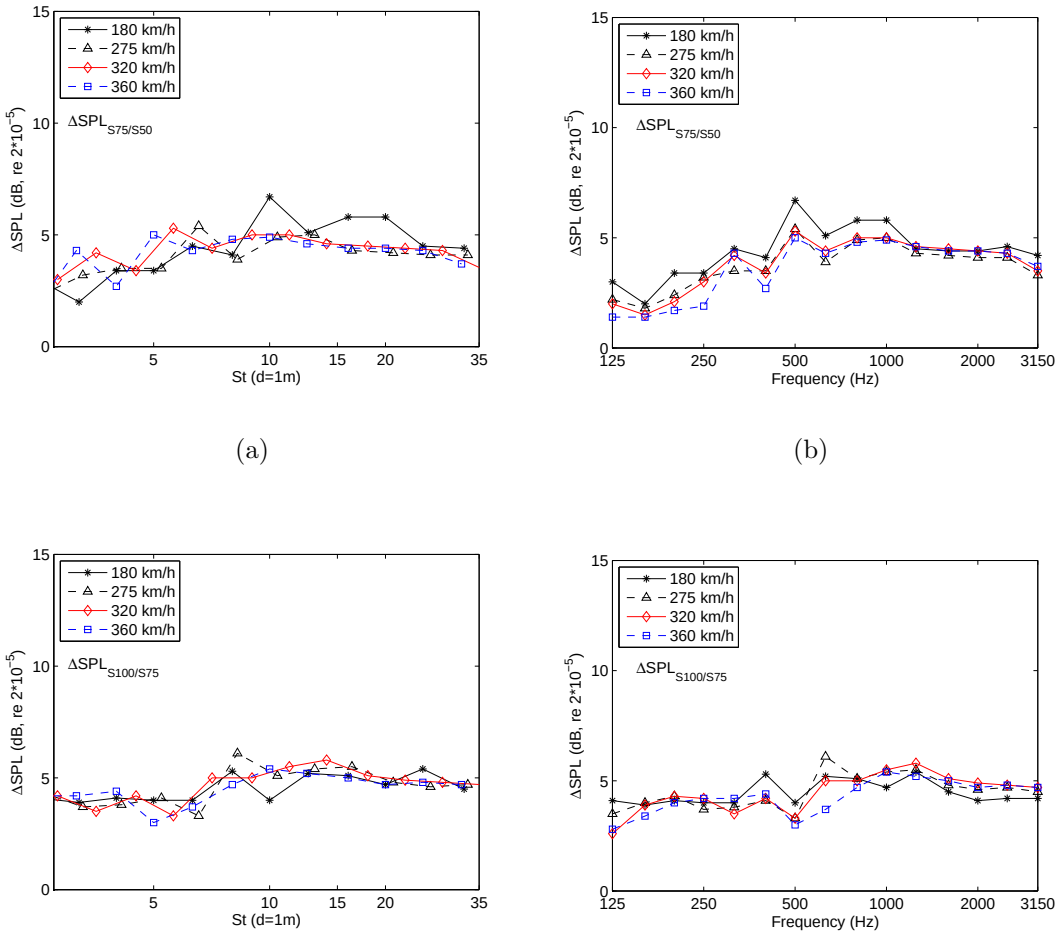

Figure 42: ΔSPL as a function of the Strouhal number and the frequency for MB+S100 vs. MB+S75 ($\Delta SPL_{S100/S75}$) and MB+S75 vs. MB+S50 ($\Delta SPL_{S75/S50}$). (a) $\Delta SPL_{S75/S50}$ against the Strouhal number. (b) $\Delta SPL_{S75/S50}$ against the frequency. (c) $\Delta SPL_{S100/S75}$ against the Strouhal number. (d) $\Delta SPL_{S100/S75}$ against the frequency.

the results it can be inferred that the speed exponent is not strongly dependent on the relative position of the bogie inside the cavity. Figure 45(b) shows the noise spectra collapsed in amplitude using a factor of $10 \times log_{10}(U)^{\alpha}$ for α equal to 6.5. The results shows a good agreement for all the flow speeds.

Figure 46(a) shows the variation of the speed exponent with the Strouhal number for the configuration MB+S100. The values are quite constant over the Strouhal number range except for the Strouhal numbers 2.5 and 5, where a minimum and maximum value are obtained. A speed exponent of 5.4 is obtained after averaging the speed exponent over the Strouhal number range. Figure 46(b) shows a good matching of the collapsed spectra using a speed exponent of 5.5.

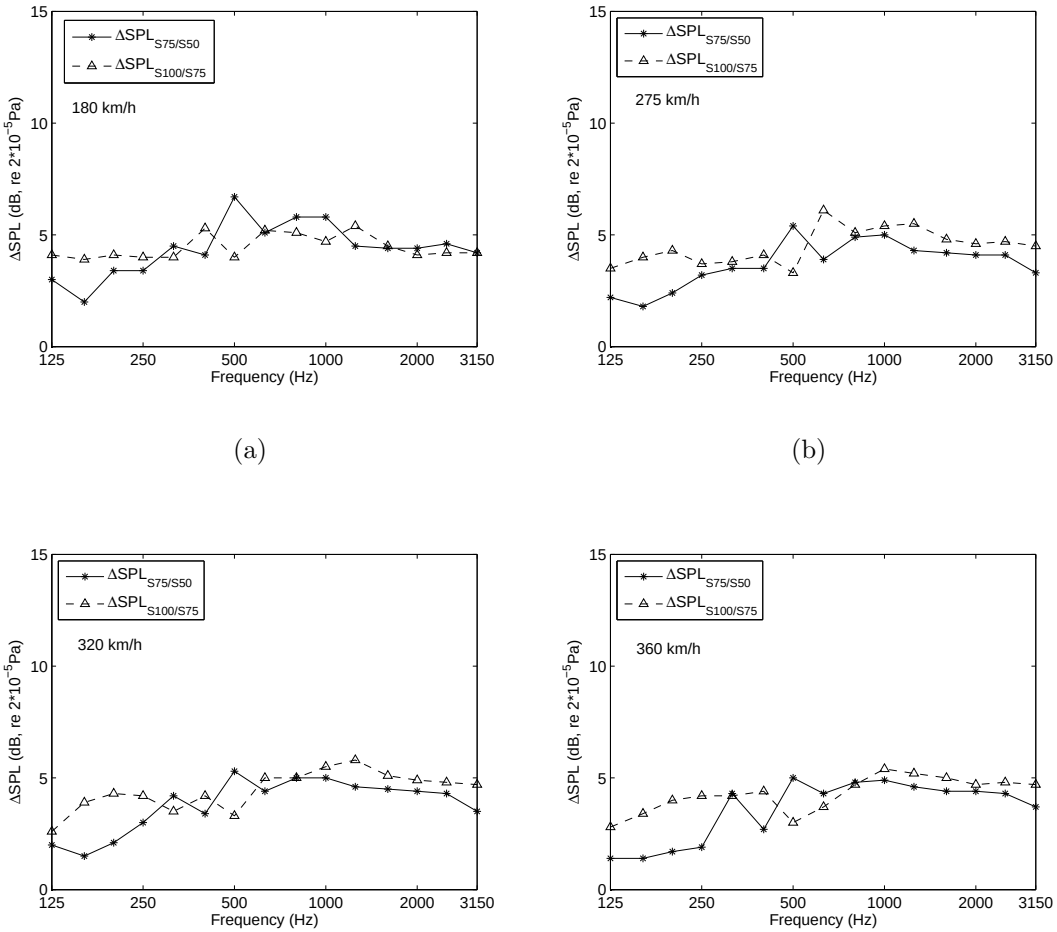

(a) (b)

(c) (d)

Figure 43: ΔSPL as a function of the frequency for MB+S100 vs. MB+S75 ($\Delta SPL_{S100/S75}$) and MB+S75 vs. MB+S50 ($\Delta SPL_{S75/S50}$) and for different flow speeds. (a) 180 km/h. (b) 275 km/h. (c) 320 km/h. (d) 360 km/h.

3.8 Directivity

For the omnidirectional microphone used in the directivity measurements, the signal-to-noise ratio for the flow speed of 320 km/h was shown in Figure 21. Nevertheless, in this case it is necessary to check if the S/N is the same for all the flow speeds. Figure 47 shows that the signal-to-noise ratio is greater than 3 dB in all the frequency bands above 800 Hz (as measured) for all the flow speeds. This is the lower limit used in the analysis of the directivity for the different flow speeds.

Figure 48 shows the OSPL measured for the configuration MB+S100 at different angles with respect to the bogie centre using different flow speeds. These data were corrected by subtracting the noise from the configuration C, which is radiated by all the noise sources present in the experiments (including the bogie cavity) except the bogie. In this case the signal-to-noise ratio was not enough for frequencies below 800 Hz. This reduction in the signal-to-noise ratio in the range between 200 Hz and 800 Hz with respect to the signal-to-noise ratio achieved with the omnidirectional microphone placed at the centre of the array when the wheels shafts were extended by 100 mm on the other side of the bogie and the noise barrier was installed (Figure 21)

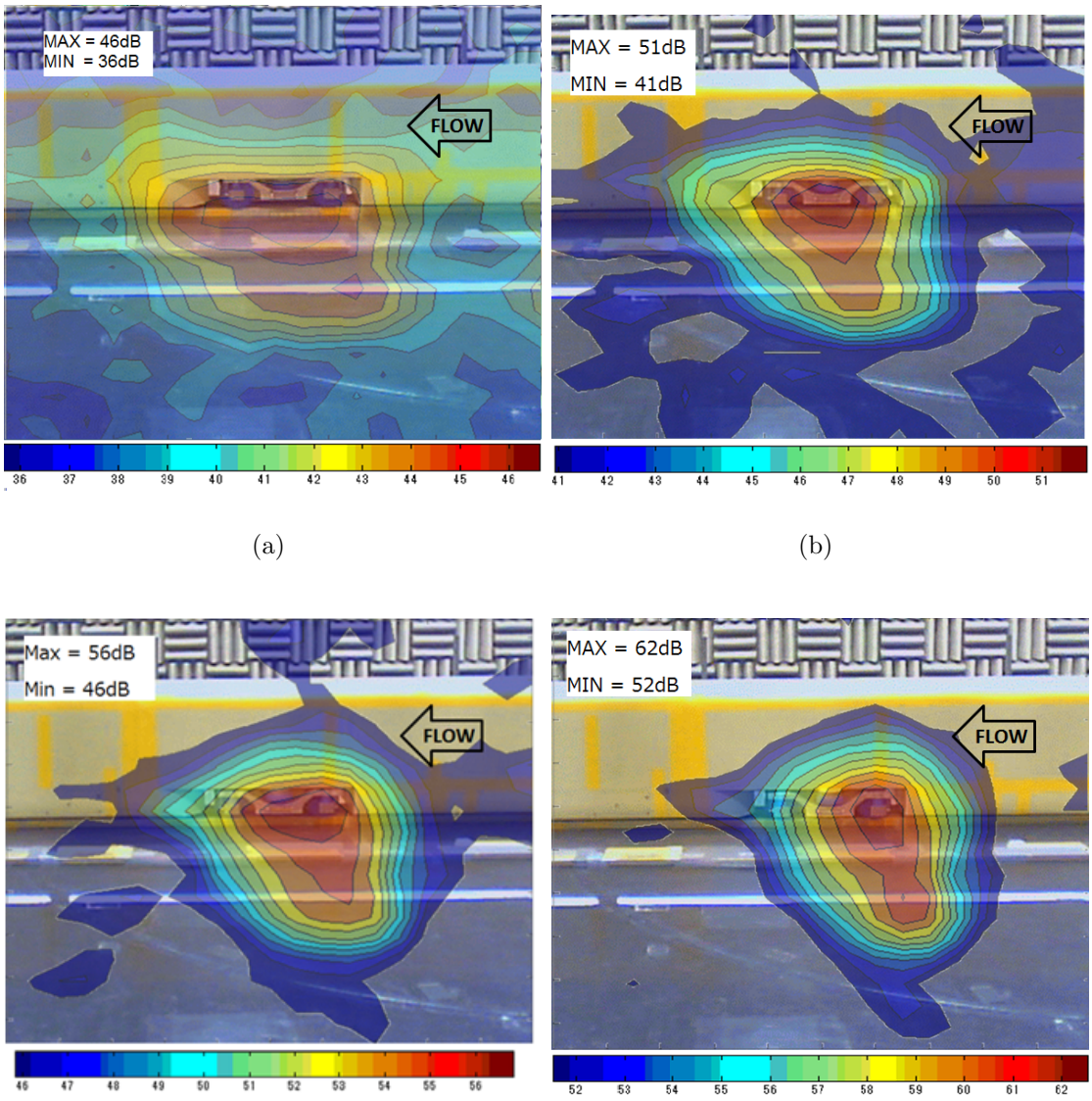

Figure 44: Noise map for the full scale 1/3 octave frequency band of 1kHz. Flow speed of 320 km/h. (a) Motor bogie standard configuration (MB). (b) Motor bogie with the side frame displaced by 50 mm (MB+S50). (c) Motor bogie with the side frame displaced by 75 mm (MB+S75). (d) Motor bogie with the side frame displaced by 100 mm (MB+S100).

can be due to the effect of the noise barrier, which was now removed, reducing the noise coming from the nose of the train.

The effect of the differences in the distance between the bogie centre and each of the microphones has been corrected using the expression $20 \times log_{10}(R_i/R_0)$ where R_i is the distance between the bogie centre and the i^{th}- microphone and R_0 is the distance between the bogie centre and the closest microphone, in this case microphone 4 with an angle of 0°. In the results shown in Figure 48 the angles for each microphone have been corrected by the convection effects using Amiet's method [6].

In order to show the results in a more reliable way avoiding any distortion that the application

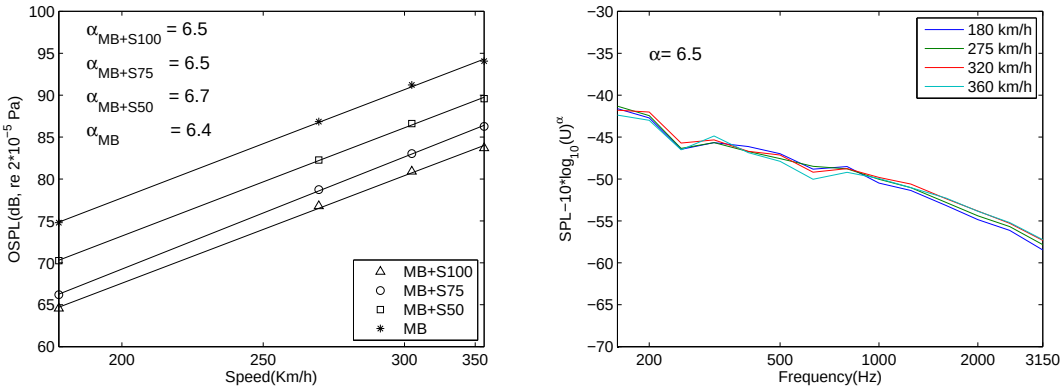

(a) (b)

Figure 45: Dependence of the OSPL with the flow speed in the frequency range. (a) Fitted results and speed exponents obtained for the cases MB, MB+S50, MB+S75 and MB+S100. (b) Data from the configuration MB+S100 collapsed in frequency using a speed exponent of 6.5.

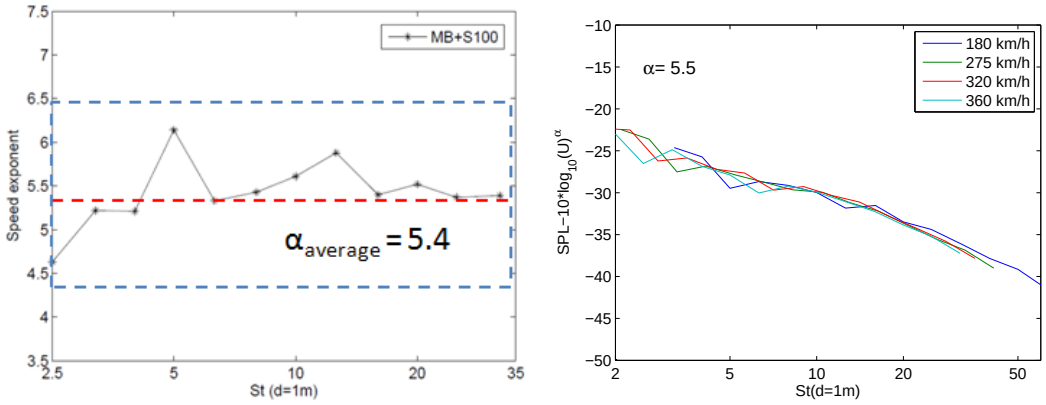

(a) (b)

Figure 46: (a) Variation of the speed exponent with the Strouhal number. (b) Noise spectra collapsed in the Strouhal number range using a speed exponent of 5.5.

of corrections may include, the changes in amplitude of the noise spectrum due to the convective amplification and due to the sound convection inside the jet and the shear layer refraction have been neglected at this stage.

It can be seen how the OSPL measured by microphone 1 is significantly lower than the OSPL measured by the other microphones and this effect increases with the flow speed . Taking the bogie as the main noise source, microphone 1 is placed beyond the theoretical limit angle (around 40° for a flow speed of 320 km/h using Amiet's method [6]) for which the sound is expected to be refracted by the shear layer preventing it from propagating out of the jet (acoustic shadow area). Therefore, the noise measured by microphone 1 may be coming from other noise sources rather than the bogie.

Looking at the results of the other microphones the differences in the measured OSPL are low and

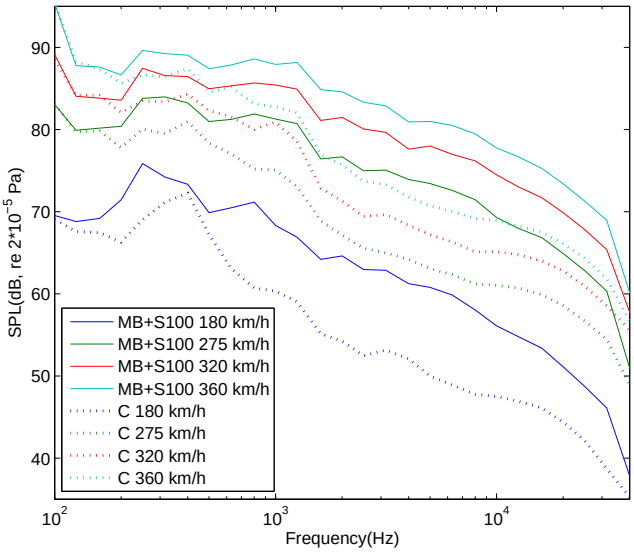

Figure 47: Comparison between the noise spectra radiated by the configuration MB+S100 and the configuration C for all the flow speeds. Frequency as measured, using omnidirectional microphones.

they look close to the results expected from an omnidirectional source. The results obtained for the flow speed of 180 km/h, which are the results where the influence of the convective amplification and shear layer refraction are lowest, show variations in the OSPL between microphones lower than 1 dB (except microphone 1 for the reason stated above). The relative difference in the OSPL between microphones seems to vary little with the flow speeds, except for microphone 2 probably due to the flow effects mentioned above, showing independence of the directivity radiation pattern with the flow speed.

Figure 49 shows homogeneity in the results of the directivity for some representative 1/3 octave frequency bands. The trend followed for each of the frequency bands is similar to that obtained for the overall SPL.

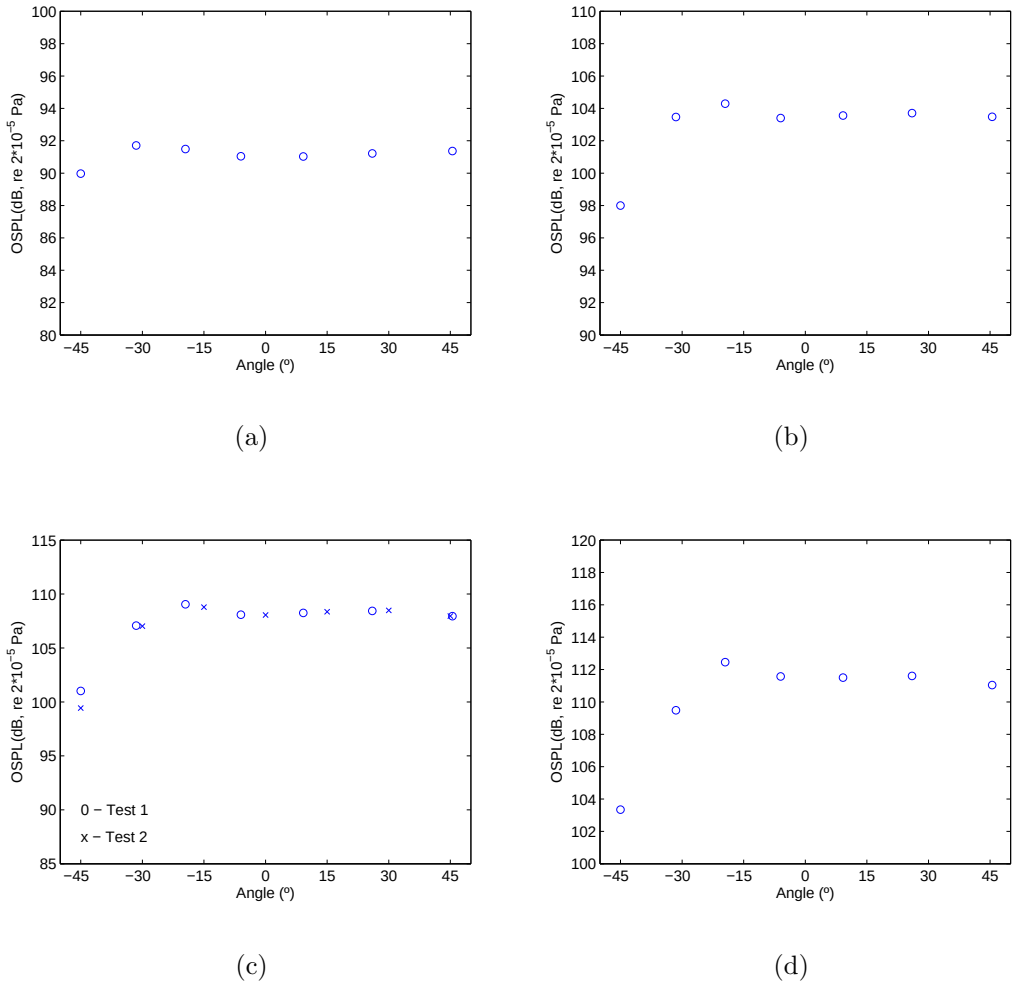

Figure 48: OSPL measured for the configuration MB+100 at different angles using different flow speeds. (a) Flow speed of 180 km/h. (b) Flow speed of 275 km/h. (c) Flow speed of 320 km/h. (d) Flow speed of 360 km/h.

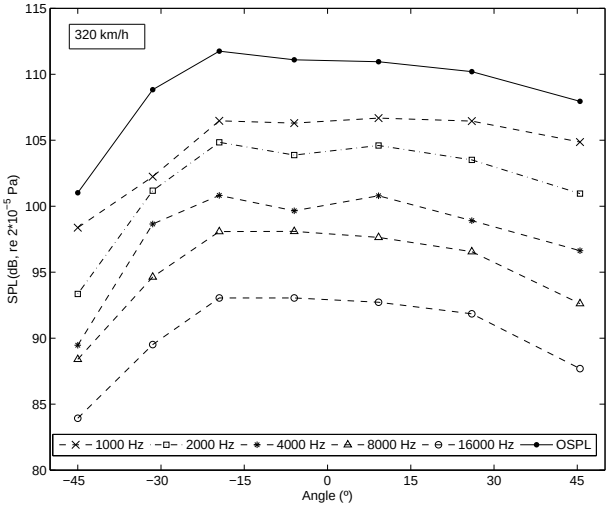

Figure 49: SPL measured at different angles for some of the 1/3 octave bands using the configuration MB+S100 and a flow speed of 320 km/h.

4 Conclusions

This report presents the results of analyzing the data gathered during the noise tests at the Maibara wind tunnel using a 1/7 scale high-speed train and bogie mock-up for flow speeds of 180, 275, 320 and 360 km/h. The conclusions presented here can be used to understand better the physical mechanisms of aerodynamic noise generation in the bogie region and also to understand how the noise radiation is related to some parameters. However the final aim of these results is, in a future stage, to use them for the calibration and validation of numerical, empirical and semi-empirical noise prediction models.

A microphone array and an omnidirectional microphone were used for the measurements. The signal-to-noise ratio obtained using the data from the omnidirectional microphone was only sufficient for the configuration MB+S100. This configuration was used for the directivity measurements due to the impossibility of using the microphone array for this in the time available to carry out these tests. The frequency range of analysis was limited to values between 800 Hz and 20 kHz (125 to 3,150 Hz full scale). The signal-to-noise ratio was considerably improved by using the data from the microphone array.

The overall noise from the bogie cavity was reduced by 3.7 dB by rounding its downstream edge. This noise reduction allowed the signal-to-noise ratio to be increased and prevented the cavity noise from masking the noise from the motor and trailer bogies.

The importance of the internal components (those located between the wheels) was assessed. When only the side frames were included inside the bogie cavity the contribution from them was negligible and the main noise source was the downstream edge of the bogie cavity. Nevertheless, when the complete motor and trailer bogie were installed the OSPL increased by 3.8 and 4.5 dB with respect to the noise from the cavity. It was found that the components or parts of components that are not shielded by the upstream step of the bogie cavity have a high contribution to the overall noise as the impinging flow speed is higher for them than for the components shielded by the bogie cavity. Therefore, the increase of 0.7 dB in the OSPL radiated by the trailer bogie with respect to the motor bogie can be explained by the increase in the surface area of the internal components (in this case the brake disks) protruding out of the shielding area of the cavity.

The use of side skirts leads to a OSPL reduction of 2.7 dB. This reduction can be explained because the skirts are acting as noise barriers for the noise sources inside the cavity (only part of the wheels are not shielded by them) and because the skirt prevents the side flow from impinging on the downstream edge of the bogie cavity and the side component of the bogie.

The effect of the bogie position along the train was studied by modifying the flow conditions at the bogie cavity inlet. Two different flow configurations were used representing those measured experimentally during field tests at the inlet of the rear bogie cavity of the first and fifth cars of a full-scale train. The horizontal and vertical flow profiles at the cavity inlet as well as a contour plot showing the flow speeds at different areas of the bogie cavity inlet were provided. The flow speed for the middle car flow configuration is generally lower at all the measurement points than the values from the leading car configuration, these differences being higher in the area between the rails. In both cases, beyond the rail the flow speed grows when the distance to the bogie centre increases and the flow is slowed down for positions close to the surfaces (ground and train floor). For the leading car case, the flow speed decreases significantly in the area between the rail and the train floor, where the wheels are located.

This reduction in the flow speed, if the middle and the leading car flow conditions are compared, turned into a reduction in the OSPL of 3.6, 2.7 and 3.8 dB for the configurations TB, MB and C. Because the highest differences in the flow speed between the middle and leading car flow configurations were located between the rails, it can be inferred that the difference in the noise radiated by the bogie when the leading and the middle car configurations are compared is mainly due to the contribution of the internal components.

The noise from the side components of the bogie was assessed by extending the bogie shafts by 50, 75 and 100 mm. The OSPL obtained for the extended axle configurations was compared with the noise from the standard bogie case MB. As expected, the OSPL rises when the surface area of the bogie components exposed to the side flow also increases. The theoretical factor $10 \times log_{10}(\Delta S)$ is able to predict the increment of the SPL with moderate accuracy: the results are underestimated by 1.5 dB. These corrections assume that the incident flow speeds remain constant throughout the surface area of all the components outside the cavity and this is not correct as was shown in the flow speed profiles. The effect of the differences in the incident flow speed depending on the component position with respect to the side of the train should be taken into account. The variation of the increase of the OSPL with Strouhal number showed that these variations are reasonably independent of frequency and flow speed.

The speed exponent was obtained for the configurations MB, MB+S50, MB+S75 and MB+S100 from the slope of the fitted function that represents the variations of the OSPL with the flow speed. Further analysis was carried out for the configuration MB+S100 because it was the less affected by the background noise. Using the speed exponent of 6.5 obtained from the procedure explained previously the noise spectra for the different speeds were collapsed in the frequency range showing a good match. The speed exponent for each of the frequency bands was calculated and plotted against Strouhal number, showing a small variability apart from the speed exponents obtained for Strouhal numbers of 2.5 and 5. An average speed exponent of 5.4 was obtained, which provided a good matching when the noise spectra were collapsed against Strouhal number. It can be concluded that the speed exponent obtained for the motor bogie noise is 6.5 if the analysis is made in the frequency domain and 5.5 if the analysis is carried out in the Strouhal number domain.

The directivity was assessed using 7 omnidirectional microphones and the configuration MB+S100 that maximized the S/N. The frequency range was limited to values between 800 Hz and 20 kHz (1/7 scale frequency range). The data presented include the correction of the noise amplitude due to the different distances between the microphones and the bogie centre and the correction of the microphone angles due to the flow convection. However, the effects on the noise amplitude of the convective amplification, the noise convection and the shear layer refraction have not been accounted for. The data show a directivity pattern very close to that from an omnidirectional noise source with a small variability with the flow speed and the frequency.

References

[1] N. Curle. The influence of solid boundaries upon aerodynamic sound. Proceedings of the Royal Society of London. Series A. Mathematical and Physical Sciences 231 (1187), 505-514 (1955).

[2] M. Iwasaki, A. Ido, N. Yamazaki, T. Uda, Y. Wakabayashi. Measurement of under-floor flow of Shinkansen train passing on slab track (in Japanese). J-Rail 2013.

[3] N. Yamazaki, A. Ido. Evaluation methods for aerodynamic noise from a high-speed train bogie in a wind tunnel test. Inter-noise and Noise-con Congress and Conference Proceedings, Osaka, Japan, 2011, pp. 1543-1553.

[4] T. Maeda, Y. Kondo. RTRI's large-scale low-noise wind tunnel and wind tunnel tests. Quarterly Report of RTRI 42(2) (2001) 65-70.

[5] N. Yamazaki et al. Prediction methods of aerodynamic bogie noise in wind tunnel tests. Proc. 7^{th} Forum Acusticum 2014, Krakow, Poland, 2014.

[6] R.K. Amiet, Refraction of sound by a shear layer. Journal of Sound and Vibration 58(4), 476-482 (1978).

A Tests schedule

Date	Configuration	Time	Flow speed [km/h]	Identifier
2013/12/16	Flow speed profiles	11:24	320	
	Micro. Array calibration	14:35	0	1
	BG	16:23	180, 275, 320, 360	13, 14, 15, 16
2013/12/17	BG+Mid	14:56	180, 275, 320, 360	39, 40, 41, 42
	C+Mid	15:22	180, 275, 320, 360	43, 44, 45, 46
	TB+Mid	15:55	180, 275, 320, 360	47, 48, 49, 50
	MB+Mid	16:32	180, 275, 320, 360	51, 52, 53, 54
2013/12/18	MB+Mid (Repeat)	10:52	180, 275, 320,360	67, 68, 69, 70
	MB	11:19	180, 275, 320, 360	71, 72, 73, 74
	C	11:37	180, 275, 320, 360	75, 76, 77, 78
	MB+S50	12:01	180, 275, 320, 360	79, 80, 81, 82
	MB+S75	13:20	180, 275, 320, 360	83, 84, 85, 86
	MB+S75 (Rep)	13:44	180, 275, 320, 360	87, 88, 89, 90
	MB+S100	14:20	360	91
	MB+S100 (Rep)	14:34	180	92
	MB+S100 (Rep)	14:48	180, 275, 320, 360	93, 94, 95, 96
	TB	15:20	180, 275, 320, 360	97, 98, 99, 100
	TB (Rep)	15:36	180	102
	TB (Rep)	15:42	180, 275, 320, 360	103, 104, 105, 106
	TB+Skirt	16:04	180, 275, 320, 360	107, 108, 109, 110
	C+Sharp	16:29	180, 275, 320, 360	111, 112, 113, 114
	FR	16:58	180, 275, 320, 360	115, 116, 117, 118
2013/12/19	Directivity C	11:38	180, 275, 320, 360	119, 120, 121, 122
	Dir.MB+S100	13:13	180, 275, 320, 360	123v124, 125, 126
	Dir C (Rep)	14:07	320	127
	Dir.MB+S100 (Rep)	14:50	320	128